Institute
of
Materials Research

51170 Köln

German
Aerospace Center

DLR

REVIEW OF AERONAUTICAL FATIGUE INVESTIGATIONS IN GERMANY DURING THE PERIOD JUNE 1999 TO MAY 2001

compiled by Claudio Dalle Donne

June 2001

1 INTRODUCTION

The review has been prepared for presentation at 2001 Meeting of the International Committee on Aeronautical Fatigue in Toulouse France, 25.-29. June 2001. German aerospace manufacturers, governmental and private research institutes, aerospace authorities as well as universities were invited to contribute summaries of aeronautical fatigue related research activities. These voluntary contributions are compiled here. The author acknowledges these contributions with appreciation. Enquiries should be addressed to the authors of the summaries.

Mailing Addresses of Contributing Companies and Institutes:

EADS-Airbus-H	EADS Airbus GmbH, Kreetslag 10, 21129 Hamburg
EADS-M	EADS Military Aircraft Business Unit, 81663 Munich
DLR-WF	German Aerospace Center DLR, Institute of Materials Research, 51170 Cologne
IABG	Industrieanlagen-Betriebsgesellschaft mbH, PO-Box 1212, 85503 Ottobrunn
IMA	Materialforschung und Anwendungstechnik GmbH, PO-Box 800144, 01101 Dresden
MTU	Motoren- und Turbinen Union, PO-Box 50 06 40, 80976 Munich
TUC-IMAB	Technical University of Clausthal, Institute for Plant Engineering and Fatigue Analysis, Leibnizstraße 32, 38678 Clausthal-Zellerfeld
TUD-IfWW	Technical University of Dresden, Institut of Materials Science, 01062 Dresden
UniBw-M	University of the Federal Armed Forces Munich, Department of Materials Science, 85577 Neubiberg
USI	University of Siegen, Department of Materials Science and Testing, 57068 Siegen
UST-ISD	University of Stuttgart, Institute for Statics and Dynamics of Aerospace Constructions (ISD), Pfaffenwaldring 27, 70569 Stuttgart
WIWEB	Federal Armed Forces Research Institute for Materials, Explosives, Fuels and Lubricants (WIWEB), Landshuterstr. 70, 85435 Erding

2 FULL SCALE TESTING

2.1 Overview of Full Scale Fatigue Tests in Germany (May 2001)

A/C Project	Customer	Test Structure	Time Schedule	Test Lab	Chapter
TANGO	EADS-Airbus	metallic and composite barrel	begin 2003	EADS-Airbus	2.2
A340-600	EADS-Airbus	center fuselage and wing	1999-2003	IMA (in coop. with IABG)	2.3
A340-500/600	EADS-Airbus	rear fuselage	01/2001-	EADS-Airbus	2.4
A340-500/600	EADS-Airbus	CFRP outer flap			2.5
AIR	EADS-Airbus	aluminum integral fuselage barrel	80 % accomplished	EADS-Airbus	
A380	EADS-Airbus	megaliner barrel	static tests 09/2001 begin of fatigue tests 02/2002	EADS-Airbus	2.7
Airbus Widebody	EADS-Airbus	cast passenger door		IMA	0
728JET	Fairchild Dornier	complete airframe	2000-2004	IABG	0
728JET	Fairchild Dornier	fuselage barrel	finished 05/2001	IMA	2.10
Eurofighter	EADS-M	wing attachment box	2001-	EADS-M	2.11
Tornado	EADS-M	main landing gear, nose landing gear	2000-2001	IABG	

2.2 TANGO Metallic and Composite Fuselage: Validation of Advanced Technologies

B. Schmidt-Brandecker, EADS-Airbus-H

The continued growth in air transport has placed an increasing demand on the aerospace industry to manufacture aircraft at lower cost, whilst ensuring the products are efficient to operate, friendly to the environment and ensure that the safety requirements are met. In frame of the fifth Framework Program of the European Union the TANGO project (Technology Application to the Near-Term Business Goals and Objectives of the Aerospace Industry) was initiated which is partially funded by the European Union. The TANGO project is the first large scale application of new technologies to achieve low-cost, low-weight primary structures. This project aims to improve the structural efficiency and reduce the manufacturing costs by achieving further reductions in airframe weight thereby lowering fuel consumption and decreasing the impact on the environment as well as lowering the acquisition cost of the aircraft by using cheaper or more efficient materials, and more efficient manufacturing processes. Furthermore the design of future aircraft structure has to consider current and forthcoming regulations as well as industry standards defined by our competitors.

The TANGO project represents an integrated approach for the validation of advanced technologies by designing, manufacturing and testing of major airframe components, i.e. a composite lateral wing box (including a metal to composite joint), a composite center wing box, a composite fuselage section and an advanced metallic fuselage section. The final results of the TANGO project will be available in 2004 and may be applied to the next generation of commercial airliners.

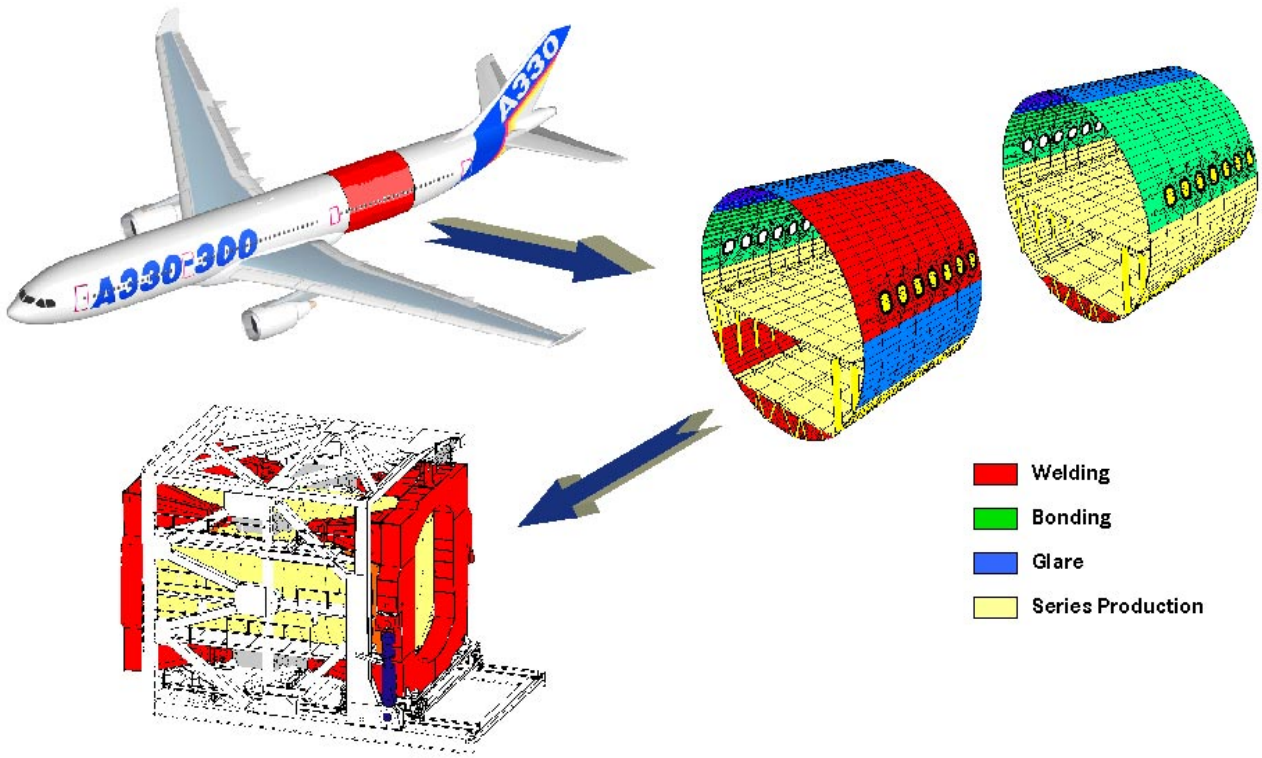

Fig. 1: TANGO Metallic Fuselage - Barrel Test.

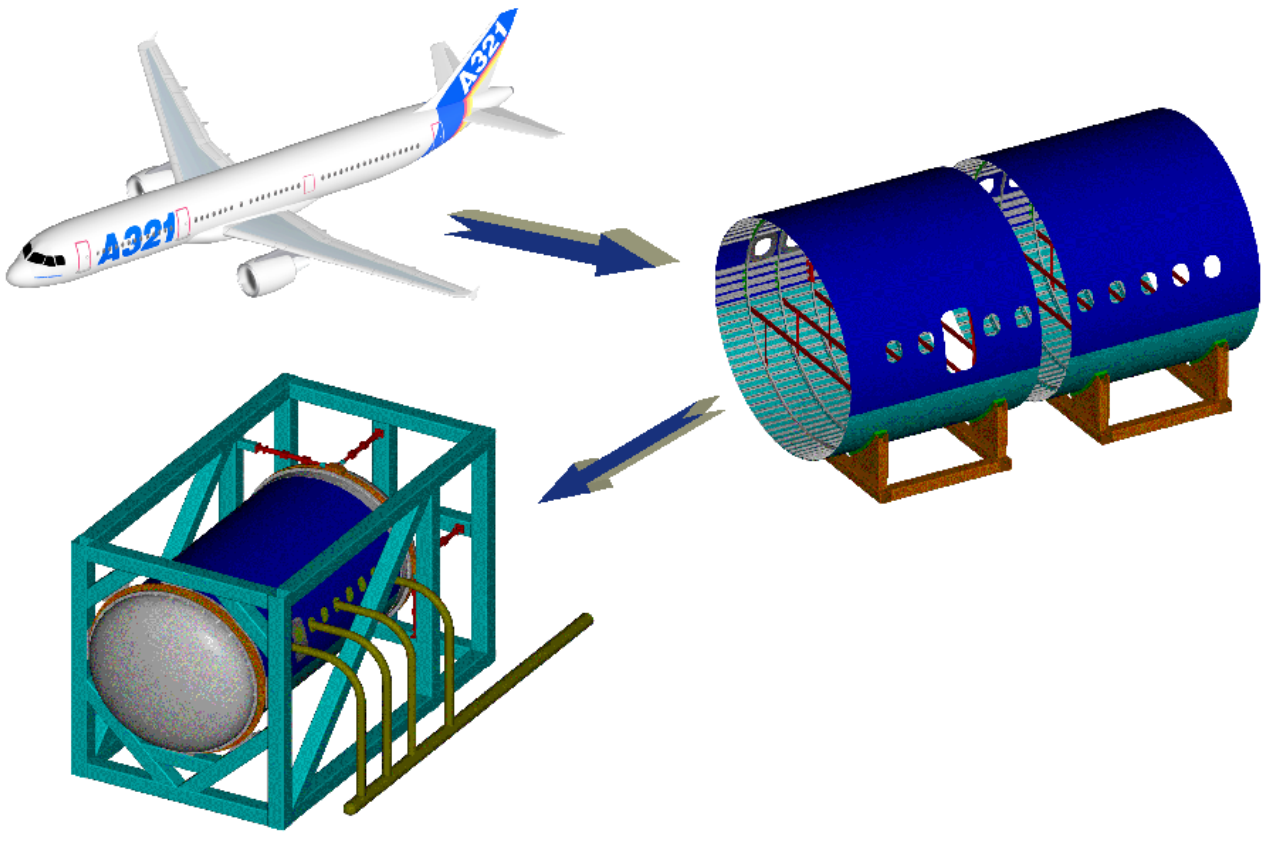

Fig. 2: TANGO Composite Fuselage – Barrel Test.

The final test within the TANGO metallic fuselage project is a full scale barrel test, see Fig. 1. The test will be based on a rear section of the Airbus A330-300 fuselage, i.e. the barrel will have the major dimensions of the A330 cylindrical fuselage and the fatigue loading spectrum will be representative of the A330-300 short range mission. The test barrel will have a length of approximately 8.5 m with a circumferential joint in the middle. The positions of the longitudinal joints are kept as in the series production. GLARE panels will mainly be located in the upper fuselage area where the advantages of GLARE may be exploited. Since the limited bearing and shear strength of GLARE does not allow to take full advantage of the superior fatigue and damage tolerance properties, new GLARE types will be investigated using alternative Al types and local higher metal volume fraction. Panels with advanced bonding technologies are located in the side shells to evaluate their capability regarding shear stresses. Welding technologies are applied mainly to panels in the lower fuselage area. There are two types of welding procedures which are very promising for aerospace application: laser beam welding (LBW) mainly for T-joints such as skin-to-stringer or skin-to-clip and friction stir welding (FSW) mainly for butt joints such as skin joints. Several materials such as 6013, AlMgLi and AlMgSc will be investigated.

The composite barrel, see Fig. 2, will be subjected to a full-scale static and fatigue test. This test will be based on the single aisle Airbus A321 regarding its major dimensions and fatigue load spectrum. The test barrel will have a length of approximately 5.5 m with a circumferential joint in the middle. Each barrel section will consist of four panels. The critical aspects to be considered in the design of a composite fuselage are: environmental effects (impact damage, lightning strike, humidity, etc.); material (damage resistance, costs and availability of a second source); certification process (crashworthiness, testing, etc.) and maintenance procedures (repairs in service, inspections methods, etc.). The design of the barrel will take into account all current certification requirements for composite primary structure. Further aspects are the external damage susceptibility which must not be worse than for the reference metallic fuselage, the repairability which should be guaranteed for each structural element and the damage tolerance requirements which should not reduce the structural strength below ultimate load capability. Advanced composite manufacturing techniques such as RTM (Resin Transfer Moulding), RFI (Resin Film Infusion) and Fibre Placement will be applied. Joining techniques will be assessed carefully in order to arrive at a cost effective assembly process. Initial manufacturing defects and non visible damages will be inflicted to the specimen prior the test.

2.3 A340-600 EF2 Full Scale Fatigue Test for Center Fuselage and Wing

Th. Nielsen, EADS-Airbus-H

The A340-500/600 Commercial Transport Aircrafts are designed and will be certified as A340-200/300 derivative according to FAR 25 Paragraph 25.571, including Amendment 45.

This review provides actual status of the EF2- test (EF2 = essai fatigue 2) program and its set-up, Fig. 3 and Fig. 4. The test installation was completed by beginning of 2001 at IMA (Material Research and Applied Engineering Ltd. Dresden) instructed by IABG (Industrieanlagenbetriebsgesellschaft mbH). With reference to the information given in the 1999 ICAF review, the EF2 test program has been adjusted to the latest requirements regarding fatigue, damage tolerance. The major topcis of the program are:

- Design Service Goal of 16600 flights,
- Verification of damage tolerance behavior,
- 10000 simulated flights at time of type certification for A340-600,
- 35000 test flights (equivalent to more than 2.5 life times), blocked in a flight-by-flight program including 10 % loads enhancement to reduce the test time,
- Loading spectrum for A340-600 typical mission representing ‘best fit’ mission mix for short, medium and long range mission,
- Min. of 16000 test flights with ”detectable“ artificial damages at A340-600 typical locations.

After transportation by Beluga transport aircraft to Dresden in February 2000 the first fuselage sections have been equipped by EADS Elbe Flugzeugwerke with test specific modifications. This comprises reinforcement doublers to attach fwd and aft fuselage pressure bulkheads and cutouts for hydraulic jacks breakthrough (e.g.). Following the delivery of the fuselage center section the fuselage join-up was performed in May 2000. The test specimen assembly was completed by attaching the two wings in September 2000. During the further set-up the test was completed by load introduction devices and the overall inspection rig. In addition the test equipment was completed by the hydraulic and pneumatic system, the data acquisition system as well.

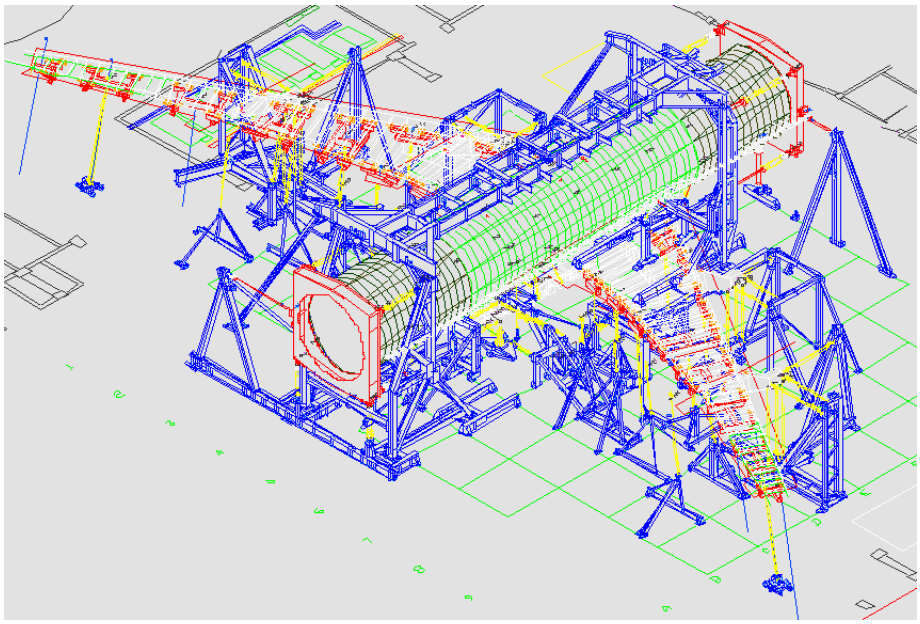

Fig. 3: A340-600 EF2 test set-up

Fig

After a commissioning phase to allow static loads calibration and in order to assess the flight test campaign a number of fatigue load cases were applied to the EF2 prior to the first flight of the A340-600. This action became necessary to represent partial limit loads since no full scale static specimen is available. With this support a full opening of its flight test envelope was achieved. Stresses were collected from about 1.500 strain gauge channels and analytical results from the finite element calculation were validated. By application of max. fatigue wing bending loads a max. wing tip displacement of 2.86 m was recorded. In addition a fuselage proof pressure test up to 821 hPa was carried out (1.33 x ΔP).

A further commissioning phase will be completed by summer 2001 to start with the calibration measurements for a large number of fatigue unitary cases. The start of the fatigue test is scheduled for beginning of September 2001 and will last about 20 month.

In parallel to the test set-up Airbus engineering departments worked out the final loads program which in general contains:

- Simulated test loads (hydraulic jack loads) with 10 % loads enhancement
- Ground steady loads (1g) with superimposed incremental loads for taxiing, turning, take-off, rotation, landing impact, landing run and braking,
- Flight steady loads (1g) with superimposed vertical and lateral incremental gust loads,
- Corresponding cabin pressure differential for each flight phase based on the typical flight profile.
- Repeated blocks of individual flight types and different severity,
- 2000 flights per block representing a randomized distribution,
- 21 flight types including 8 different airborne sub-flight types and 3 different ground sub-flight types are foreseen,
- Random application of flight types and load cases.

It is foreseen to complete the test by a detailed analysis of the test structure, i.e. to run a tear down program scheduled to start in April 2003.

2.4 Airbus A 340-500/-600 – Rear Fuselage Section (18/19)

I. Malm, EADS-Airbus-H

Within the framework of the certification of A340-500/600 Airbus, fatigue tests are being performed with a rear fuselage section in the Structure Test Center of the EADS Airbus GmbH, Fig. 5.

These tests were necessary because the type of construction of the rear fuselage section compared with the A340-300 type has been modified in a considerable way, especially in the area of sections 18/19. Essential characteristics of these changes were, among other things, the elimination of the strut system for pick up of the vertical stabilizer loads in the area of section 19 as well as the introduction of a pressure bulkhead made of carbon fiber composite, which considerably increased the space available behind the pressure bulkhead and, of course, resulted in a weight reduction.

The structural component to be tested includes, as already mentioned, sections 18 and 19 with the pressure bulkhead, the passenger and the cargo compartment decks and two passenger doors. At the front end of section 18, restraint doublers are applied over a frame bay to ensure a soft transition from the rig to the test area. In this area, the test specimen is rigidly connected with the test equipment.

The structural components installed in the area of the rear fuselage section, e.g. vertical stabilizer, horizontal stabilizer and tail cone were developed as dummy structures and connected to the structure to be tested with all original fasteners. Thus, a representative stress was ensured.

The loads are applied on the fuselage via two hydraulic jacks, one of which acts in the pressure area on the passenger deck (32 load points) and the other on the tail cone dummy. In the vertical stabilizer area, a total of 18 hydraulic jacks were arranged in such a way that the required loads resulting from gusts and maneuvers can be applied. Four hydraulic jacks act on the horizontal stabilizer. The internal forces resulting from the different material expansion coefficients of the interconnected structural components (metal fuselage, stabilizers of carbon fiber composite) during temperature changes are taken into account during load simulation.

And, of course, the cabin is also loaded with an internal pressure corresponding to a certain cruising altitude.

At first, the loading program included a series of static measurements, structural stresses were determined in exposed areas at relevant flight load cases. Afterwards, a total of 60000 flights are to be simulated. The load program includes, in

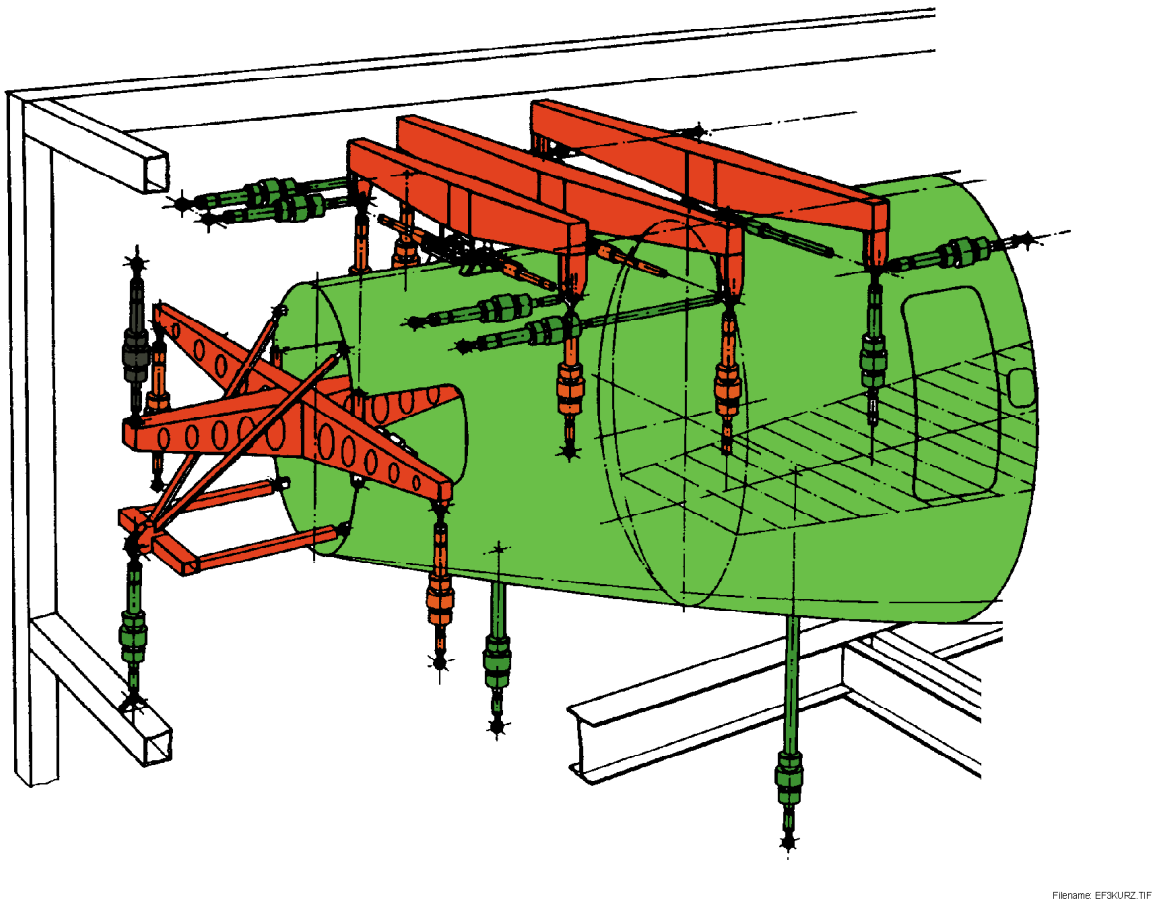

Fig. 5: A 340-500/-600 rear fuselage section test setup.

a block of 1660 flights, 8 different flight types (A – H) whose duration and load level (amplitude) are of varied intensity. Thus, an flight type A includes approximately 1000 different load points and is seldom simulated, whereas an flight type H includes approximately 90 load points and is often simulated.

Since the beginning of the tests in January 2001, about 8000 flights have been simulated (State: April 2001).

After performance of 60000 flight the tests will be completed with ultimate loads.

2.5 Full-Scale Fatigue Tests on A340-500/600 Outer Flap

V. Bruns, EADS-Airbus-H

For certification of the Airbus A340-500/600, full-scale fatigue tests at room temperature (RT) are being performed on a LH outer flap to demonstrate sufficient fatigue and damage tolerance behavior. These tests are carried out at the EADS-Airbus GmbH (Structure Test Center, Hamburg).

The flap structure mainly consists of CFRP. In load introduction areas, fittings made of milled Al alloy are installed. The CFRP structure had been damaged artificially during production to obtain initial defects resulting from manufacturing processes, e.g. bonding failures, tool impacts etc. No moistening prior to the fatigue tests was carried out. This stiffness influence is obtained by factoring the simulated air loads, Fig. 6.

The flap is supported at three stations by carriage- and track-dummies and is fixed in one position. The test loads (representing aerodynamic loads) are introduced into the lower surface by elastic pads. Loads resulting from wing bending are introduced by the middle track station, which can move vertically, and by the cruise roller at inboard and outboard end rib.

A total of fifteen servo-hydraulic jacks are used to introduce the loads of the test program. The air loads representative of three flap positions are simulated at intervals of 5000 flights. These loads are generated in a process-computer and controlled by digital control units .

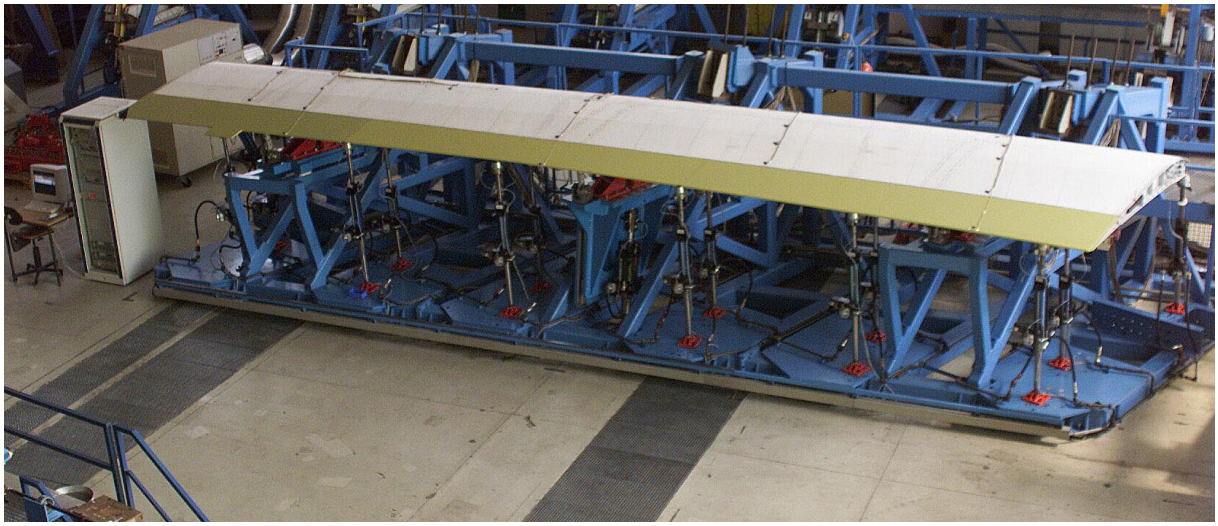

Fig. 6: Test setup for fatigue– and damage tolerance tests on A340-600 outer flap.

The fatigue tests are to provide information on the following:

- behavior of the initial manufacturing defects
- potential fatigue areas
- damage tolerance behavior
- efficiency of different repair methods.

Visual and ultrasonic inspections of the test structure are performed at regular intervals.

The stiffness of the entire flap will be measured ten times during the fatigue tests. Until now no new damage, damage propagation or change in the stiffness have occurred.

At the end of the fatigue tests, a residual strength test will be carried out on the damaged structure.

2.6 Full Scale Testing of a Cast Passenger Door

W. Entelmann and N. Ohrloff, EADS-Airbus-B

The casting technology offers the potential for primary aircraft structures to combine reasonable mechanical strength at reduced weight and lower costs. A possible application of this technology is a passenger door structure integrated at multiple locations in the aircraft at identical design. Consequently the number of parts to be cast efficiently from a single tool is high for an aircraft family, resulting in development and test of an Airbus 'Widebody' door structure. The component is a single-piece sand cast part (D357) with the outside skin machined to loft contour. A casting factor of 1.0 has been applied in the design. With a size of 2100x1100x125mm and the thickness of the structural elements from 1.5 to 5mm (skin/web of inner structure) the cast prototype exhibits a weight of 56kg. Coupons were cut from the first castings to check the material properties which denotes to 270/ 330MPa for yield/ultimate tension strength and a minimum elongation of 5%. In addition fatigue and damage tolerance properties were investigated. Comparison of fatigue test results performed on plane/notched specimens (K_t=1.0 and 2.5) in the as-cast condition with specimens repaired by welding (with subsequent heat treatment) revealed no degradation due to the welding process. The crack growth tests on CCT specimen showed a crack growth at R=0.1 equivalent to 2024-T3.

A Full-Scale Fatigue Test device for the cast door structure was established at the IMA test institute in Dresden to check the fatigue performance under realistic internal pressure loading, see Fig. 7. The test setup consists of a welded steel pressure box closed by an original door cutout panel of a widebody aircraft. The cast door installed in this rig can be loaded via a computer controlled pressure system. During the test phase 4 major repairs were installed and some accidental damages like impacts and scratches were made. 11 saw cuts in the cast structure and one door stop failure were made after 40000 cycles. After conclusion of the fatigue cycling at 120000 Δp cycles neither natural fatigue cracks nor any extension of the initial saw cuts were found. One artificial damage in the skin was extended several times up to a length of 90mm but even for this length no crack initiation was found after 31400 cycles.

The good structural integrity of the door after simulation of 120000 cycles enables additional static tests. The static strength at 2xΔp was tested on the intact structure and with one door stop missing. Limit load internal pressure 1.15xΔp

was applied with 2 door stops missing and in a second case with a 260mm long crack above a broken beam (all door stops in place). Neither failure in static tests nor crack extension during residual strength test was observed.

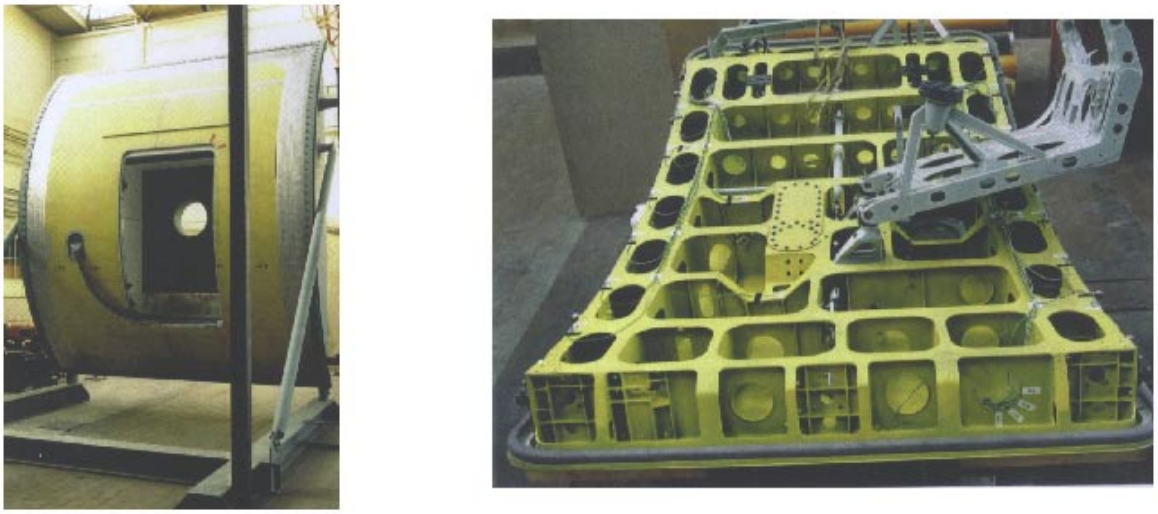

Fig. 7: Cast passenger door and test equipment.

2.7 Structural Testing of Megaliner Barrel

T. Müllert, R. Hinrichs, M. Wagner, EADS-Airbus-H

The transport of 500 to 1000 people in one aircraft requires the design of a pressurized fuselage with two passenger decks. Compared to a circular fuselage with one deck, the loads of the horizontal and vertical tail plane must be carried through two decks up to the wing. The upper floor can not be supported by additional struts. If lateral loads have an effect on the fuselage, an unsymmetrical deformation will occur. Also internal pressure loading will cause an extraordinary deformation.

These deformations cause a very complex stress distribution and are therefore are an uncertainty in the design of a 'megaliner' with regard to fatigue and damage tolerance capabilities required in the regulations FAR/JAR 25.571. A large scale fatigue test has to be carried out to investigate the potential technical risks. This should reduce the economical risks for the manufacturer and the airlines. Further the application of advanced materials and designs and the reduction of weight by designs which are not applied by now has to be investigated.

The major objectives of the fatigue test program for the Megaliner Barrel are:

- apply realistic loads especially regarding the lateral deformation,
- detailed measurements of stresses and deformations,
- to provide test data for life predictions and to verify the predictions,
- to locate early identifications of any fatigue critical areas for modifying structures,
- crack propagation and residual strength investigations to verify the goals airworthiness and maintenance,
- verification of the behaviour of new designs, new materials and new production methods,
- create data as a basis for the design of an aircraft with comparable dimensions

On account of the exceptional dimensions of the test specimen, which represents the rear fuselage section from frame 56 to frame 80 (height: approx. 9m, width: approx. 7m, length: approx. 15m, see Fig. 8), accommodation of the test setup in one of the existing test hangars was not possible. That is why the test rig was installed outside the test hangars and was simply covered with weather and noise protection panels (see Fig. 9). Accommodation of the test supply systems and of the measurement and control systems is provided for in a supply hangar and a control station adjacent to the test rig. The test will be monitored by a video system.

Besides utilization during the tests, the test rig is also used as a mounting frame for the test specimen. After equipment of the test rig with the manufacturing equipment necessary for barrel assembly, the barrel will be assembled from a total of 18 fuselage sections. Assembly is scheduled for the time period from May to September 2001.

For the tests, both ends of the test specimen will be connected to pressure bulkheads. One pressure bulkhead will be rigidly connected to the test rig, the other will be loaded with 8 hydraulic jacks depending on the loads at section to be adjusted. For correction and/or realistic introduction of the side loads, eight hydraulic jacks will be installed laterally along the test specimen transfer the loads to selected cross beams and frames of the barrel. For load simulation through freight and passengers, the cargo, main and upper decks will be loaded with a total of 14 hydraulic jacks acting in Z direction of the test specimen. Loads will be introduced onto the decks by means of whiffle trees with extensive branching in order to ensure a realistic load distribution.

Before the beginning of the intended fatigue test, approximately 25 static load cases will be applied on the test specimen and the strains, deformations and forces will be measured at a total of 2000 measurement points.

The simulated test loads represent:

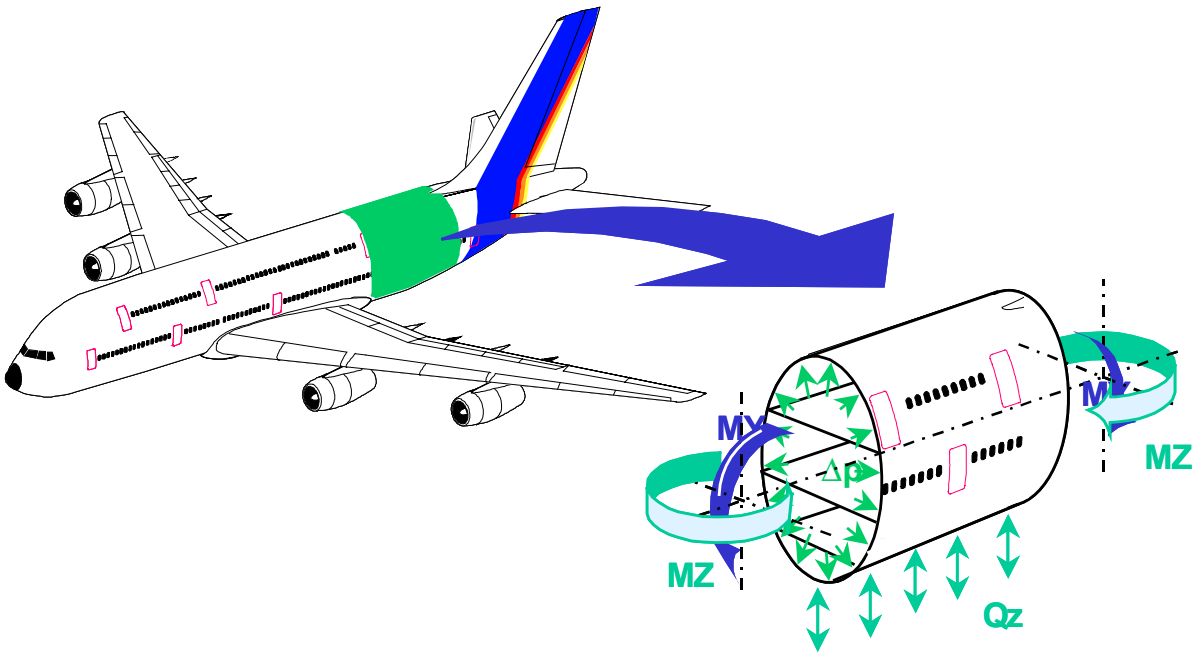

Fig. 8: Location of the barrel in a ’megaliner’.

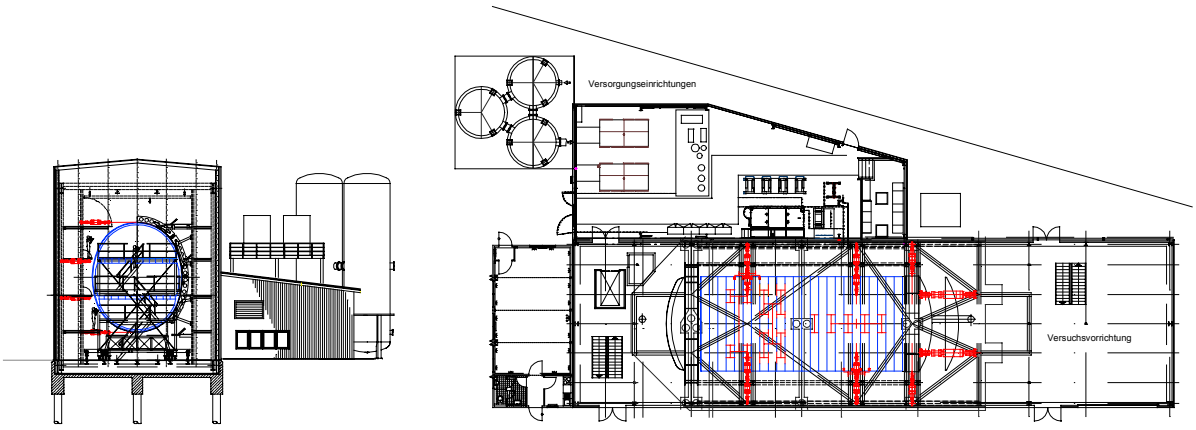

Fig. 9: Schematic diagram of the Megaliner Barrel test set-up.

- ground loads: 5 basic loads (1g) with superimposed incremental loads for take off run, rotation, touch down, landing roll and taxi in.
- flight loads: 11 basic loads (1g) with superimposed incremental loads for vertical and lateral gust.
- corresponding cabin pressure differential for each flight phase based on typical flight profile.

The test program represents

- 28 blocks and 2150 flights per block representing a randomized distribution.
- 8 flight types of different severity.
- Random application of flight types and load cases.

A number of standard repair solutions and artificial damages will be selected and installed on the test specimen to investigate the fatigue and damage tolerance behaviour.

2.8 Full Scale Fatigue Tests with GLARE Fuselage Shells

T. Beumler, EADS-Airbus-H

The introduction of fiber metal laminates as fuselage skin material in civil transport aircraft requires an investigation of the consequences for a full scale fatigue evaluation. Aircraft manufacturers have collected significant experiences with monolithic aluminium structures in the past. Time dependent degradations of the metal are linked to corrosion, a damage type which will be covered by a dedicated inspection task for the aircraft fleet. A variable which can be accounted for in the full scale test is the mission mix. The mix of short, long, severe and less severe test flights should represent the average utilization expected in service. A conservative component can be included by truncating the peak loads, which otherwise would increase the fatigue life due to local plastification effects. Temperature effects do not need to be considered for monolithic aluminium parts. Both, crack initiation and crack propagation properties of aluminium, are almost constant above the freezing point and even increase below it. A full scale test conducted at room temperature is conservative for aluminium parts, since substantial portions of the in-service flight loads will appear during cruise, at very low temperatures.

A full scale specimen should be manufactured under exactly the same conditions as the aircraft, in order to test a representative manufacturing quality. The remaining factor to be considered for the interpretation of full scale test results for aluminium structures is the material scatter. Airbus is conducting at least two life times fatigue tests with ten percent increased load levels. The method is aiming for 95% probability of survival, i.e. not more than 5% of the aircraft parts should be subject of fatigue damages before reaching the Design Service Goal. Widespread fatigue damage is not allowed throughout the entire life, to be verified by the tear down inspection at the end of the test.

Structural items are evaluated regarding fatigue and damage tolerance for certification and are included in the Airworthiness Certification Document (ACD6). The number of flights until the fatigue crack becomes detectable, divided by a material scatter factor, determines the inspection threshold. The crack propagation period is considered to be short compared with the crack initiation period. For that reason, the threshold determination is conservative, i.e. the structure should have no or very small damages at the time of first inspection. Concluding, the scatter factor for monolithic aluminium structures in a full scale test article is the scatter factor for crack initiation, see Fig. 10.

GLARE is a hybrid material containing two components with different stiffness and different coefficients of thermal expansion – aluminium and glass fibers. The prepreg matrix is epoxy based, thus susceptible to moisture absorption.

Extensive investigations on the crack initiation behaviour of GLARE at different temperatures have been conducted by Delft University. Similar as for monolithic aluminium, the crack initiation is postponed at negative temperatures, compared with room temperature. Crack initiation at both, room temperature and higher operational temperature (70ºC) is equal.

Crack propagation is temperature dependent, with increasing temperature cracks propagate faster. Comparative crack propagation calculations with different temperature profiles, superposed to a short range stress spectrum, have been conducted. An entire mission, calculated with da/dN-data representative for room temperature, has been compared with a skin material temperature profile, which considered 80ºC for all ground and the early flight cases, -50ºC during cruise and room temperature during descent and landing. It was observed, that the low crack propagation rates at cruise overcompensate the high crack propagation rates at high temperature.

For both cases, crack initiation and crack propagation, a full scale test conducted at room temperature is conservative for GLARE. The influence of ageing on both properties is under investigation. However, due to the internal stress system, the aluminium layers in GLARE crack earlier than in monolithic aluminium at the same applied load. After initiation,

cracks propagate very slow due to the crack bridging of the fibers. Small cracks at multiple sites are tolerable as long as the ultimate load can be transferred.

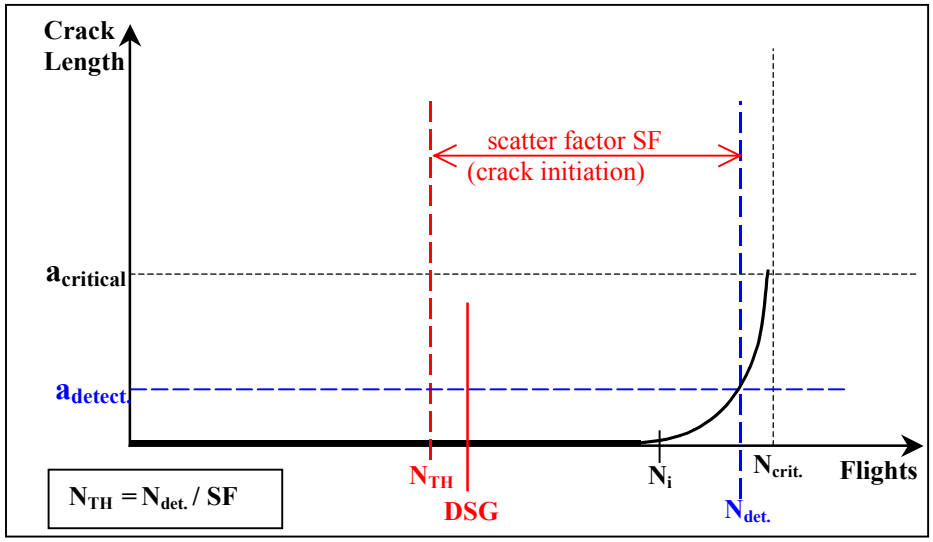

N_i: flights to crack initiation, N_{det}: flights to detectable crack length, N_{crit}: flights to critical crack length

Fig. 10: Determination of inspection threshold for aluminium riveted joint. The scatter factor is related to crack initiation (fatigue).

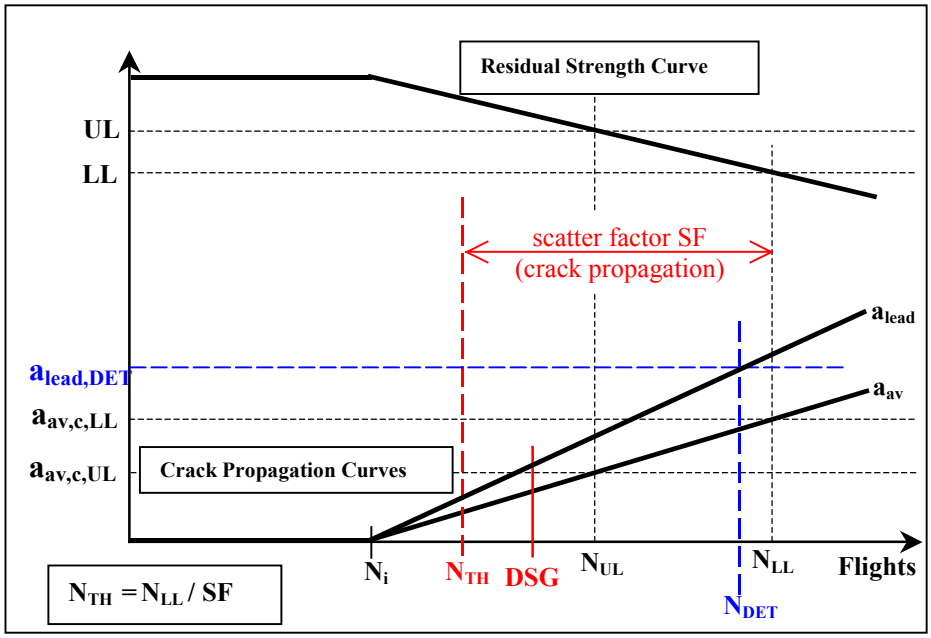

UL: ultimate load, LL: limit load, a_{av}: average crack length, a_{lead}: lead crack length, $a_{av,c,UL}$: crit. crack length (ultimate), N_I: flights to crack initiation, N_{UL}: flights to ultimate load capability, N_{LL}: flights to limit load capability

Fig. 11: Determination of inspection threshold for GLARE riveted joint. Ultimate load capability is given at DSG. No directed inspection required, although calculated inspection threshold reached prior to Design Service Goal. The scatter factor is related to crack propagation.

The safety level for aluminium structures, must be equal for the GLARE structure. However, when the cracks initiate earlier and the crack propagation phase is longer than for monolithic aluminium, a crack propagation related scatter factor has to be evaluated for GLARE, see Fig. 11. In fact, the residual strength in GLARE can decrease so gradual, that still at the end of the full scale test the ultimate load can be carried. In this case, no inspection is required.

2.9 Fairchild Dornier 728JET Full Scale Fatigue Test

W. Sutter, IABG

In September 2000 IABG has been contracted to perform the full scale test campaign on Fairchild Dornier´s 728JET. In the scope of this task the full scale static test set up as well as the full scale fatigue test set up are presently being designed and will start operation in 2002. This review briefly outlines the full scale fatigue test CF1 (Certification Fatigue 1).

The purpose of the CF1 is to qualify the primary structure of 728JET with regard to fatigue and damage tolerance behavior in accordance with FAR/ JAR 25.571. Thus a Flight-by-Flight Load Spectra simulating a total of 200.000 flights will be applied to the specimen whereas 100.000 flight cycles will be accomplished during the fatigue testing phase and another 100.000 cycles will form the damage tolerance phase after application of artificial damages. The total load spectra will represent a design life of 80.000 flights at a scatter factor of 2,5.

The test specimen will consist of:

- fuselage
- wingbox structure including engine pylons, all flap tracks and flaps, 1 slat, 1 Krüger Flap, 2 spoilers and both ailerons
- vertical stabilizer including rudder
- main and nose landing gear, engines, APU and horizontal stabilizer will be represented by dummy structures

As a peculiarity the flaps will be driven under load as to provide configurations matching each flight phase.

The basic loading concept for the CF1 as well as the maximum loads for each of the 49 hydraulic loading cylinders and the pneumatic loading system for fuselage pressurization have already been frozen in February 2001. Presently the loading rig is being designed and its assembly will start in October 2001. Subsequent to integration of the specimen (beginning in February 2002) pretests are scheduled for June 2002. The actual test operation for fatigue and damage tolerance assessment will begin in September 2002 and require approximately two years.

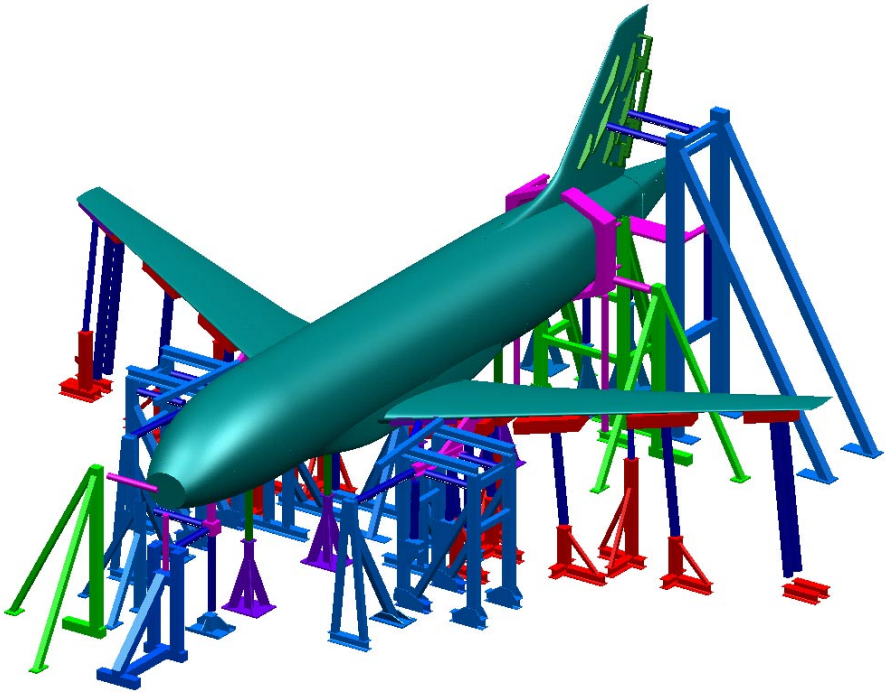

Fig. 12: Loading concept for 728JET Full Scale Fatigue Test.

2.10 728JET Fuselage Barrel Test

M. Semsch, D. Schönfeld, IMA, H. Hickethier, Fairchild Dornier

A fuselage barrel fatigue development test was performed at IMA GmbH Dresden and terminated succesfully recently (May 2001). The test specimen represents a fuselage section from behind the wing of the Fairchild Dornier 728JET (dimensions: length = 4090 mm, diameter = 3470mm). It consists of 10 fuselage center skin segments, where each segment is built up with different structural configurations. The primary aim of the test is to get a final decision on the fuselage design. For this purpose

- the fatigue properties,
- the damage tolerance,
- the residual strength and
- the risk of wide spread fatigue damage

of the structure are determined.

The test was designed as a full scale test, which includes a flight-by-flight test program of a flight mission with

- 13 different flights,
- 100 load cases and
- and test goal of 200.000 simulated flight hours.

The test set up (see Fig. 14) allows to simulate tension, bending, torsion, shear and internal pressure. The barrel is loaded by 4 independent servo-hydraulic jacks. The cabin pressurisation is realised by a pneumatic system.

The fatigue test was finished successfully. In the damage tolerance test phase, various artificial damages were introduced in the structure. The results of the measured crack propagations (see example in Fig. 13) will be used to define possible inspection intervals and methods.

2.11 Wing Attachment Box Fatigue Tests

A. McCarthy, EADS-M

The Wing Attachment Box (WAB) fatigue test program forms a major contribution to the qualification route for the Eurofighter centre fuselage wing attachment structure with special emphasis on the major frames, carbon fibre composite (CFC) skin and fuel tanks.

An additional goal of the test is to qualify the damage tolerance of the laser welding manufacturing technique for the intake duct Al-Li panels. The LH intake duct is manufactured using the Nd-YAG laser welding process for incorporation of stiffening ribs whereas the RH duct skin incorporates integrally machined ribs. Hence a comparison of the performance of both techniques can be made.

The test is being performed at the EADS Structural Test Laboratory in Ottobrunn, Germany.

The WAB incorporates the aft centre fuselage which includes the three major attachment frames and the CFC outer skin. Wing loads are introduced into the frames by left- and right- hand wing dummies. To adequately simulate fuselage

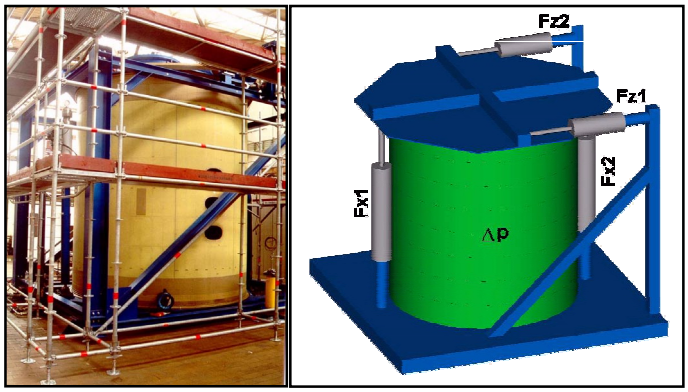

Fig. 14: 728JET Fuselage Barrel Test rig.

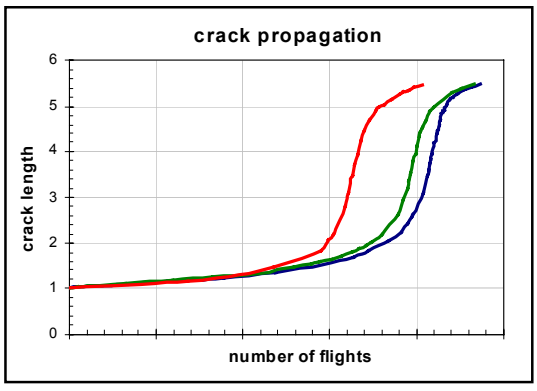

Fig. 13: Example of crack propagation measurements of artificial damage.

bending, a portion of the rear fuselage is included and loaded by an actuator and gantry simulating rear fuselage and engine vertical inertia effects. The structure is further extended forwards to a built-in frame where all forces are reacted into the test rig. Additional longitudinal loading is applied to the forward two main frames to simulate the restraint across the landing gear bay normally provided by the wing. Furthermore rigid rods are installed longitudinally between the wing dummies for the same purpose.

A randomised flight-by-flight test program of 18000 Simulated Flight Hours (SFH) will be performed to verify the required 6000 operational flight hours (scatter factor of 3).

Manoeuvre load cases with fuel tank pressures (using water) as well as ground operations will be simulated.

Environmental conditions are taken into account in so far that the fuel tank water is systematically heated to 95°C during the program to simulate the recovery temperature effects on the CFC skin.

Verification of the structural Finite Element Model (FEM) is an essential requirement of the test measurements and to this end a total of 730 strain gauge channels and 40 deflection transducers are attached and will produce the data for the evaluation of the structure. Static and dynamic measurements up to maximum loads in the fatigue spectrum are included in the program.

Static tests with local fuselage centre pylon store loads will also be performed.

Impacts of various intensities are applied to CFC components at high stressed areas of the longerons, frame flanges, ply drop off areas and one access cover. Using ultrasonic equipment these areas will be monitored throughout the test to substantiate the damage tolerance requirements.

Structural inspections will be conducted at selected intervals during the fatigue testing phase in accordance with the inspection procedures.

Applied actuator loads are monitored by load cells and compared with supply values.

Fuel tank pressures are monitored by pressure transducers and achieved temperatures by thermocouples.

The control system embodies closed loop digital servo controllers addressed by a host computer to command each loading channel simultaneously.

Following completion of fatigue testing up to 18000 SFH, certain static load cases will be taken to 80% ultimate design load at elevated temperature to demonstrate the required residual strength.

Finally, selected load cases will be taken to 100% design ultimate load at room temperature and one case taken to failure.

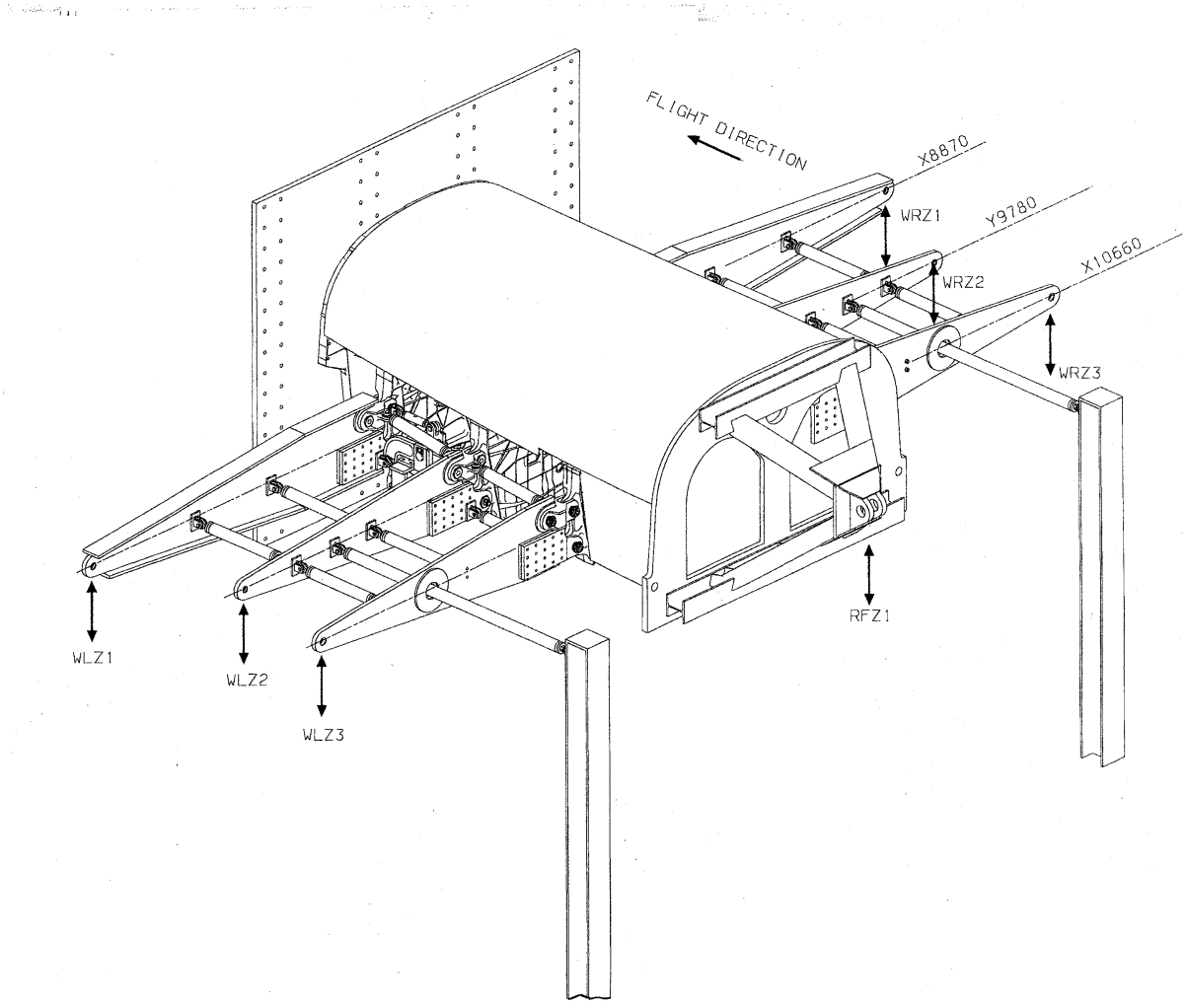

Fig. 15: Schematic of Eurofighter wing attachment box fatigue test set up.

3 FATIGUE AND FRACTURE OF FUSELAGE PANELS AND JOINTS

3.1 Damage Tolerance Tests of Plane and Curved Panels

S. Goldbach, G. Kaiser, A. Keiser, IMA

The damage tolerance behaviour of plane and curved fuselage panels was examined in the national program "Rumpf neuer Technologie (fuselage of new technology)". Different material for skin and stiffeners (2014, 6013, 2524, various types of Glare, several heat treatments), joining methods between stiffeners and skin (riveting, bonding, welding as well as integral extrusions were investigated. The servo-hydraulic test rigs are shown in Fig. 17 (the curved fuselage panel test rig was described in the 1999 Review).

The crack growth of 14 plane panels, Fig. 16, was investigated under pulsating tensile stress. The crack started from a mechanical saw cut of the type "crack above broken stringer". The residual strength test was performed after the final crack length reached two stringer spacings ("two-bay-crack"), Fig. 18.

In the tests of twelve curved fuselage panels, Fig. 17, the crack propagation behaviour of longitudinal and circumferential cracks in the skin as well as cracks above a broken stiffener were tested under flight-by-flight spectrum. The circumferential cracks were repaired after reaching the final crack length of a "two-bay-crack". Subsequently the crack propagation tests of longitudinal cracks in the skin and also above broken frames were carried out. The residual strength test were performed with longitudinal cracks above a broken frame, Fig. 18.

To achieve continuous crack growth in the GLARE laminate unbroken glass fibers in the crack wake had to be cut.

Within the contest of this review, a short summary of the results is not possible because of the wide variety of parameters investigated. From a damage tolerance point of view C188 and GLARE show a better behavior than 6013 and 2024.

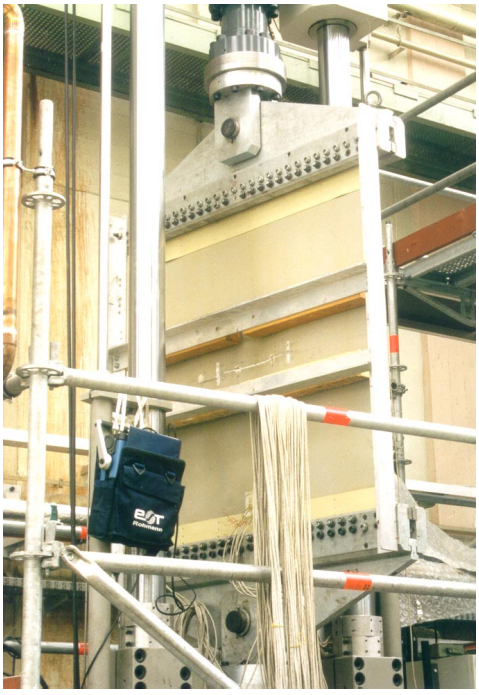

Fig. 16: Test facility for plane panels.

Fig. 17: Test facility for curved fuselage panels.

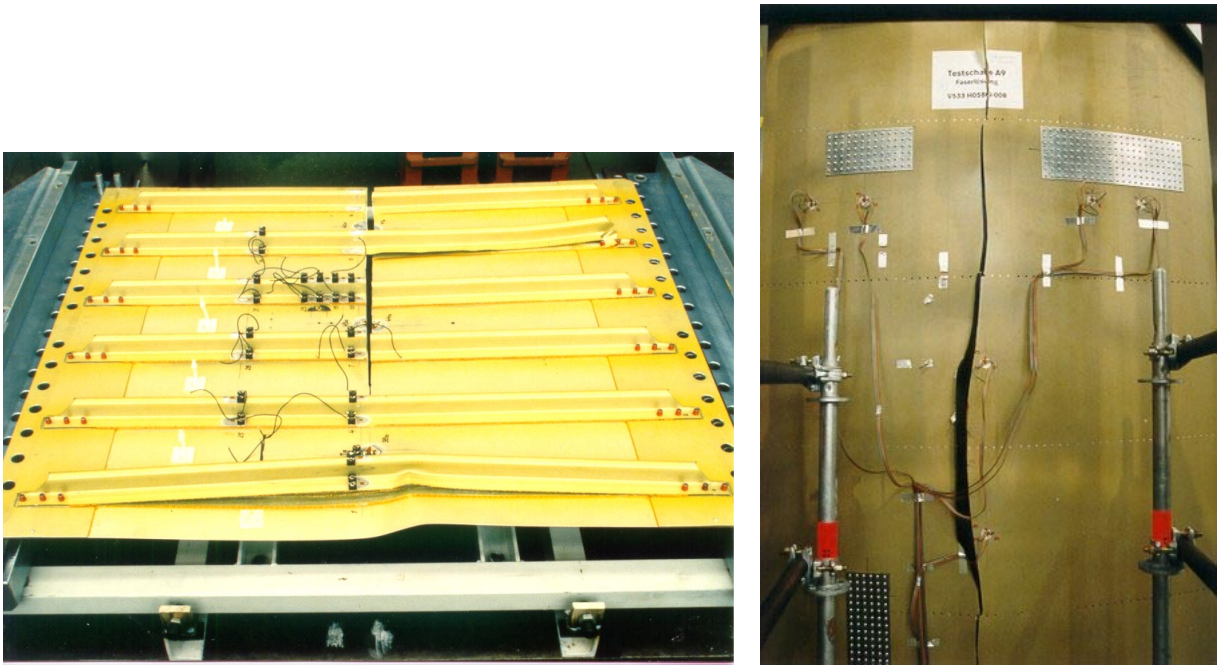

Fig. 18: Plane and curved test panels after residual strength test.

3.2 MSD Tests with A300-Fuselage Panels

S. Goldbach, G. Kaiser, A. Keiser, IMA

In the “Aging Aircraft” program fatigue and damage tolerance tests were carried out with 4 curved fuselage panels, two of them after lifetime. The test panels consisted of 2024-T3 skin material with bonded stringers. Two panels had a longitudinal lap joint and two panels had longitudinal and circumferential lap joints, Fig. 19.

In the IMA fuselage panel test facility the following parts of testing were carried out:

Fuselage panels with longitudinal lap joint:

- fatigue life of the structure up to failure loaded by constant amplitude internal pressure
- propagation of a longitudinal crack in the skin up to defined crack length, constant amplitude loading
- residual strength test with natural cracks in the lower rivet row of the inner panel

Fuselage panels with longitudinal and circumferential lap joint:

- flight-by-flight fatigue loading up to failure
- flight-by-flight fatigue up to defined crack length
- residual strength test with natural cracks in the inner rivet row of the splice plate

The critical locations for natural crack initiation were:

- the lower rivet rows in the longitudinal and circumferential lap joint especially in the covered skin layer
- the inner rivet row of splice plate of circumferential lap joint and the lower rivet row of inner panel.

To detect the damage the multiple frequency and magneto-optical eddy current testing as well as the ultrasonic testing methods were used.

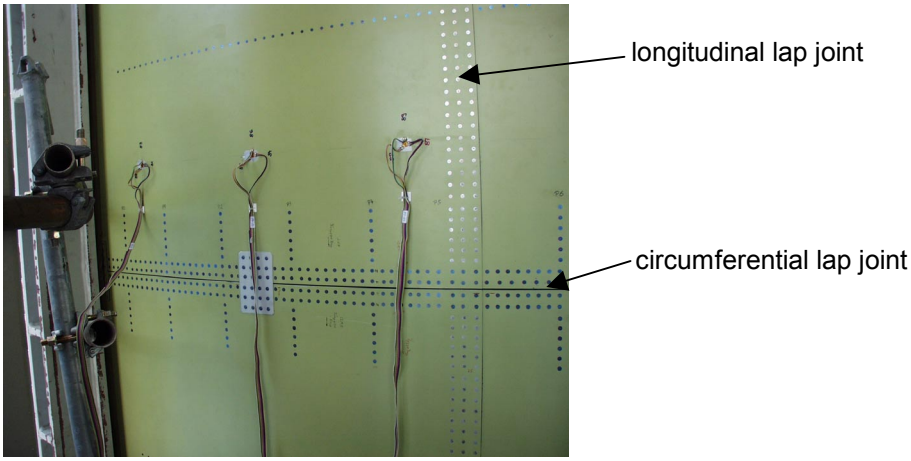

Fig. 19: Inspection area of the curved A300 aging aircraft panel installed in the IMA test facility.

3.3 Fatigue of Friction Stir Welded Butt Joints

C. Dalle Donne, DLR-WF, G. Biallas, Univ. of Paderborn

In a DLR core research project butt joints in the thickness range from 1.6 mm to 10 mm of 2xxx and 7xxx series aluminum alloys have been produced using the friction stir welding (FSW) technique. With a part of these joints microstructural, mechanical and corrosion characterization studies were carried out [1-6].

The static strength is always equal or higher than 80 % of the ultimate strength of the base material. The drop of the S-N fatigue strength of the joints compared to the parent material is also in the range of 20 %, when specimen with polished surfaces or with a very smooth fingerprint of the FSW tool shoulder are investigated. Lower fatigue strengths are usually associated with a bad surface finish and a weld toe, which is left behind by the FSW tool shoulder.

At low R-ratios, fatigue crack propagation curves of friction stir welded joints show an specimen geometry effect which is related to the different residual stress distribution in the specimens. After machining of the specimens from the butt joints, compressive residual stresses were present at the crack tip of a C(T) specimens whereas tensile stresses were active at the crack tip of a M(T)-specimens. These residual stresses alter the true load ratio in the specimen and have therefore an effect on the da/dN-ΔK-curves. On the basis of the K_{eff}-approach and a simple residual stress measurement it is possible to remove the residual stress effects from the test data. The da/dN-ΔK_{eff} curves of the base material and the

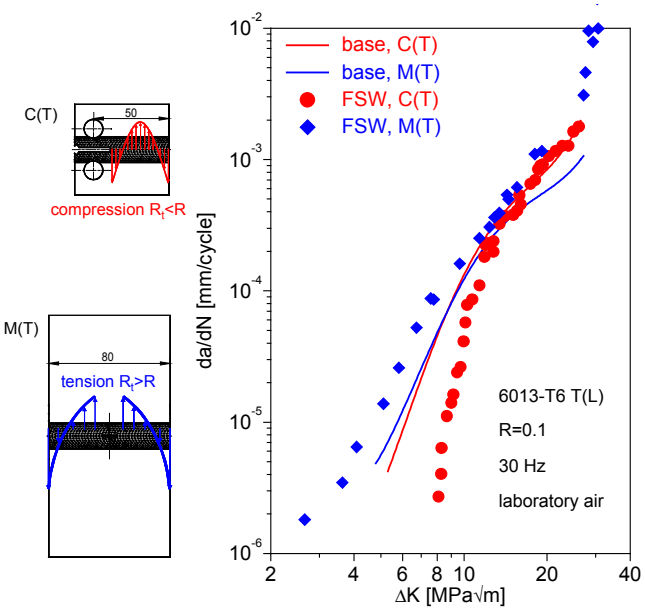

Fig. 20: Influence of specimen geometry on nominal da/dN-ΔK curves of FSW joints.

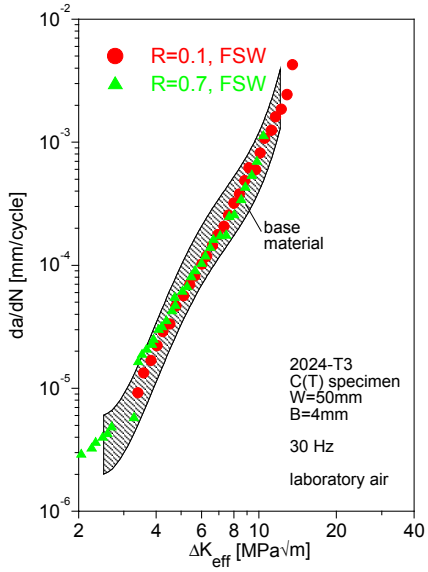

Fig. 21: The effect of residual stresses and R-ratio of on da/dN-ΔK curves is suppressed if the crack propagation rates are plotted as a function of the effective stress intensity factor range ΔK_{eff}.

friction stir welds then fall in a common scatterband, i. e. the true material properties of base material and FSW joints are very similar.

3.4 Static and Fatigue Tests with CFRP Bolt Joints

W. Fessenmayer, M. Lieback, IMA

On behalf of EADS Airbus, IMA GmbH Dresden carried out static and fatigue strength tests with CFRP bolt joints. Aim of these tests was to assess design rules of a CFRP outer wing of a Megaliner.

Following parameters were varied [7]:

- specimen thickness and design
- bolt diameters and materials
- joining techniques
- load transfer
- bending

Static and fatigue loads were introduced by means of a hydraulic test rig with forces up to 1000 kN. Strains were measured to determine the load transfer. Strain gauges as well as an optical measurement system were used for this purpose. The optical system is based on the optical raster method and provides an image of the strain distribution on the surface, Fig. 22.

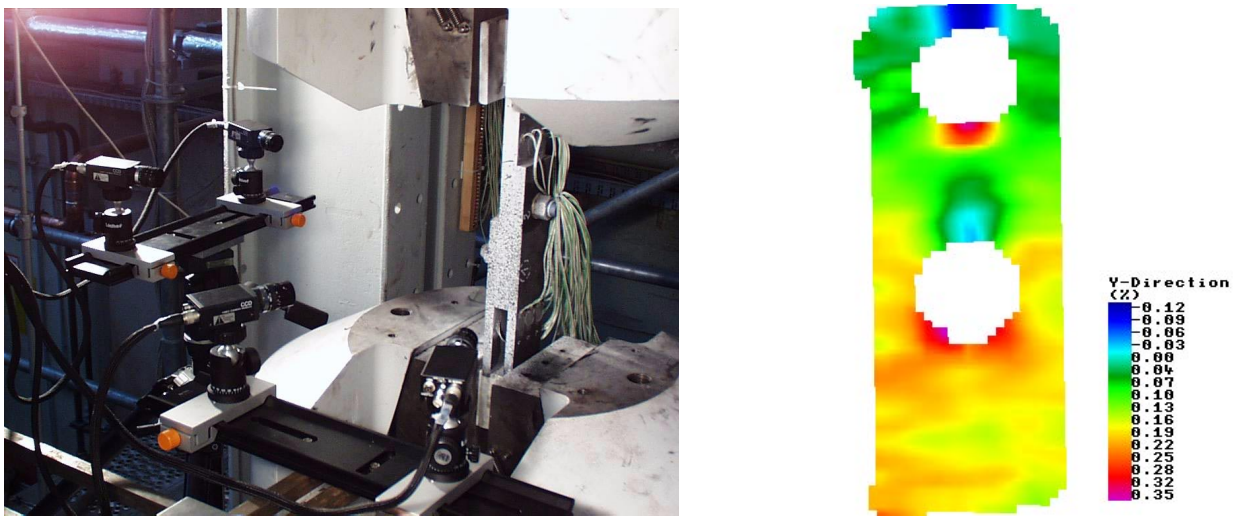

Fig. 22: :Test set-up with bolted specimen and optical measurement system (left) and strain distribution on the specimen surface (right).

4 FATIGUE LIFE ASSESSMENT AND PREDICTION

4.1 Influence of Cut-Out Size on the Inspection Threshold for Skin Repairs

H. Assler, EADS-Airbus-H

The Repair Assessment Guidelines (RAG) outline specifications for damage tolerance and static strength assessment of repairs and establish requirements for repairs that may need supplemental inspection. The main objectives of the document are

- to provide a practical methodology to allow repairs to be evaluated by operators,
- to direct the repair evaluation process and
- to develop a repair evaluation process for required inspections (e.g. threshold, interval).

To estimate the inspection threshold for a riveted skin repair at a pressurized fuselage a simple equation, that represents a factored fatigue life, can be applied. Several factors are used to take into account the influence of global location, local secondary bending, riveting (type, diameter, pitch of fastener) and material, to name a few. One of these factors is SC (size of cut-out) that reflects the influence of the cut-out size on the inspection threshold. In the case of a small cut-out the load is partly transferred by the doubler and partly redistributed to the adjacent skin area which results in a higher fatigue life of the repair.

Both experimental and theoretical investigations were performed. The experiments included nine tests of flat unstiffened panels with different sizes of cut-out ($S_{cut,longitudinal}$ = 66-1298mm, $S_{cut,circumferential}$ = 154mm). The specimens were tested at a constant stress ratio (R=0.1) and amplitude in longitudinal direction and the time to crack initiation (TTI, a=0.25mm) was monitored.

The numerical investigation is primary based on a finite element analysis to calculate the stress field, especially in the riveted area where the doubler is fixed to the skin. In a second step analytical functions were applied to determine local stress concentrations near to the rivet holes (bypass, bending, pin-load). As shown in Fig. 23 a stress concentration occurs at the corner of doubler which results from the local increase of stiffness (overlapped area). The estimation of the TTI is based on the assumption that the TTI of every single rivet hole varies statistically and can be described by the Gaussian distribution. As a consequence two different types of failure occur:

Type I: The threshold is limited by the high stress concentration which is applied to a small number of rivet holes at the corner of the doubler.

Type II: The threshold is limited by the weakest rivet hole (probabilistic approach) which is applied to a relative low load concentration (in comparison to the rivet holes mentioned above).

Fig. 24 represents a diagram that is proposed to estimate the SCI-factor with respect to the size of cut-out ($S_{cut,c}$, $S_{cut,l}$). The scatter of the experimental results indicates that only a combination of both experimental and theoretical investigation enables a better insight in the numerical behavior. In addition to that it is shown that usually a variation of cut-out size in circumferential direction $S_{cut,c}$ has a more significant influence on the threshold compared to the cut-out size in longitudinal direction $S_{cut,l}$. This is based on the fact that the longer $S_{cut,c}$ is, the more load will be attracted (high stress

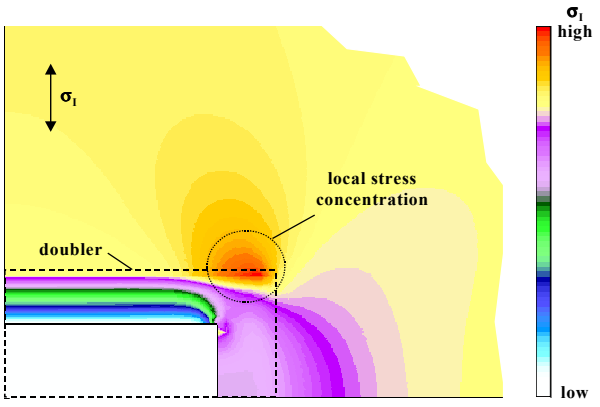

Fig. 23: ¼-Model of skin repair (hidden doubler).

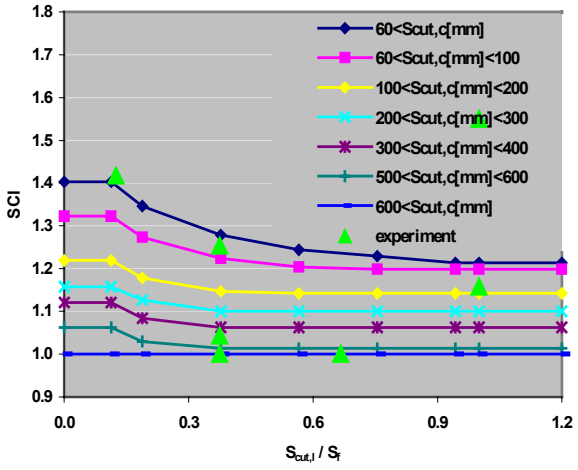

Fig. 24: Size dependent SCI-factor (S_f: frame pitch)

concentration at the corner of the doubler) whereas an increase of $S_{cut,l}$ leads only to a longitudinally shifted zone of stress concentration.

Based on this approach the inspection threshold and interval could be determined in the following for both skin and doubler.

4.2 Analysis of Structures Potentially Susceptible to Widespread Fatigue Damage

H. Trey, EADS-Airbus-H

Following the well known Aloha accident in 1988, where the presence of small cracks at adjacent fastener holes (Multiple Site Damage, MSD) in a skin lap splice led to in-flight structural failure of the upper part of the forward fuselage, international activities have been launched (Airworthiness Assurance Working Group (AAWG), Industry Committee on Widespread Fatigue Damage (WFD)) to ensure continued structural airworthiness of ageing aircraft. As a result of these activities the AAWG submitted a report entitled 'Recommendations for Regulatory Action to Prevent WFD in Commercial Airplane Fleet'. In an European Research Project (SMAAC) a methodology to assess WFD/MSD has been developed that follows the recommendations provided by the AAWG. This methodology is now used in frame of the A300 Life Extension Programme to assess the behaviour of structural items in the presence of Multiple Site Damage (MSD). The methodology has been enhanced, validated by extensive comparison and testing.

The methodology is based on a Monte Carlo Simulation of multiple crack initiations to generate initial cracking scenarios followed by a deterministic calculation to calculate crack propagation and failure for each scenario. The method is summarized as follows :

1. Each potential crack location (e.g. two sides per fastener hole in a lap splice) is allocated a crack initiation time. The initiation time is determined by randomly drawing a "live" from an overall log-normal distribution of fatigue lives for simple coupons
2. The propagation of each initiated crack is calculated by linear elastic fracture mechanics, where the stress intensity factor is calculated by a compounding procedure. Plasticity effects are accounted for by considering Irwin's plastic zone in front of each crack tip.
3. Failure of the structural items is estimated by some pre-defined condition, such as growth to a predefined crack length, exceeding a critical stress intensity factor or an R-Curve technique to estimate residual strength.

These stages form a single Monte-Carlo iteration and are repeated many times to form a complete Monte-Carlo simulation of the structural item under investigation.

Significant improvements have been achieved recently in three major parts of the method, namely (a) the damage accumulation procedure, (b) the determination of stress intensity factors used for compounding and (c) the residual strength calculation.

a) The damage accumulation procedure accounts for the influence of stress redistribution due to the occurrence of cracks on the crack initiation. Here, three main effects are considered : the increase of net stress, the stress increase at the uncracked side of a cracked hole and the stress increase at an uncracked hole adjacent to a cracked hole. The increased accumulation of damage due to these effects leads to earlier crack initiation at the considered locations.

b) Furthermore, the stress intensity factors used within the compounding procedure have been enhanced. Special emphasis has been laid on corner cracks as well as on interaction of different types of cracks – an important phenomenon in each multiple crack configuration. Additionally the linkup process of adjacent cracks has been investigated in greater detail by comparing various link-up criteria such as touching plastic zones (Swift criterion) or net section ligament failure. From comparison to tests it can be stated that the net section ligament failure leads to conservative results, while the criterion of touching plastic zones gives slightly unconservative estimates in some cases.

c) A correct estimate of the residual strength of a component in the presence of MSD is needed to complete the WFD analysis. Therefore, a R-curve procedure has implemented, which accounts for crack interaction. In this procedure each crack tip of a simulated crack scenario is investigated for unstable crack extension.

As a result of these improvements this method is now capable to accurately simulate the behaviour of complex structural items such as longitudinal joints. Extensive comparisons to test results derived from the Airbus WFD Testing Programme as well as from Full Scale Fatigue tests have been done to validate the predictions. Fig. 25 presents one of the results of the WFD test programme, where a severe MSD scenario – a combination of 0.127 and 1.27 initial cracks – has been tested (red/yellow lines) and simulated (blue line).

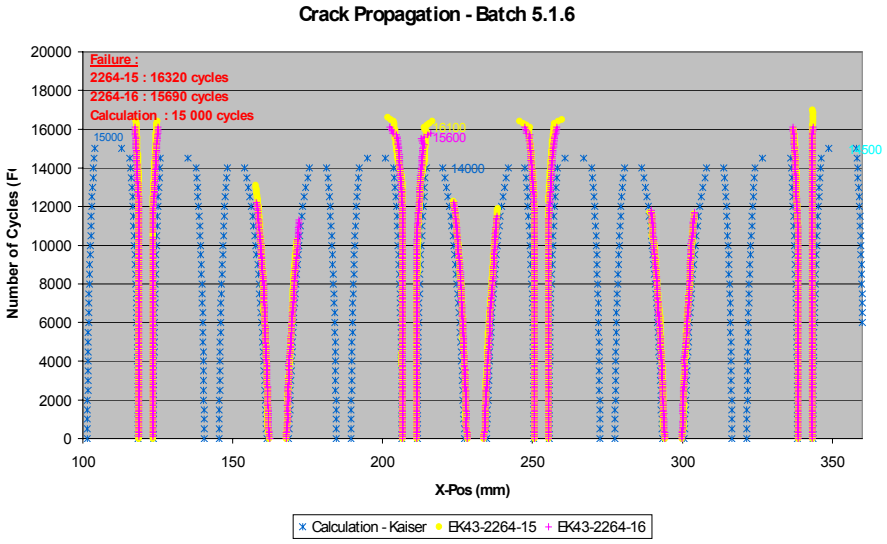

Fig. 25: Comparison of predicted (blue) and measured (red/yellow) crack propagations in a WFD test.

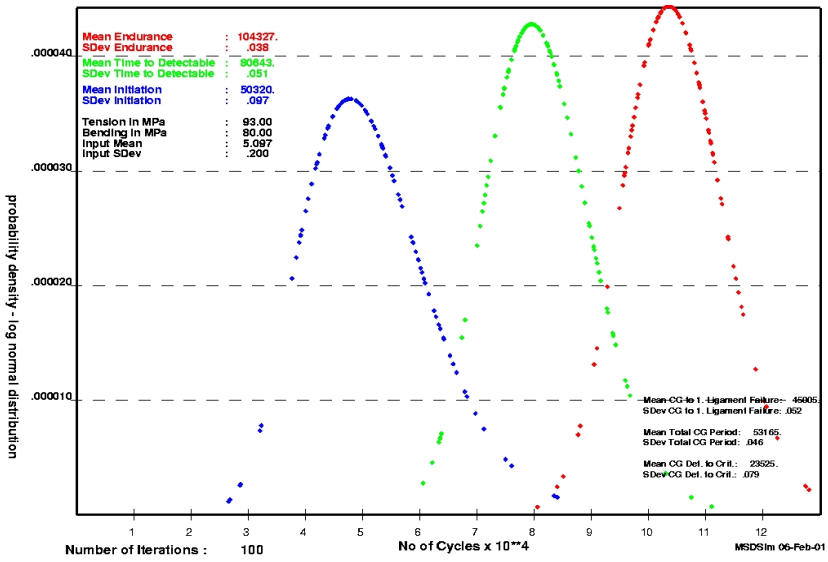

Fig. 26: Example of Time to Crack Initiation (blue), Time to Detectable (green) and Time to Failure (red) probability distributions.

As stated above this simulation method is now used in the A300 Life Extension Programme to obtain maintenance programmes for structural items susceptible to WFD. This programme is based on results obtained from a complete Monte Carlo Simulation. These results are presented as probability distributions for certain points in the life of a structural item, namely the Time to Crack Initiation, Time to Detectable and the Time to Failure. An example of the corresponding graphical output is shown in Fig. 26, where the blue, green and red lines represent the Time to Crack Initiation, Time to Detectable and Time to Failure, respectively.

4.3 Developments in the program CRACKTRACER

G. Dhondt, MTU

The program CRACKTRACER is software which enables the user to calculate cyclic crack propagation with the finite element method. The core of the program consists of algorithms which insert an arbitrarily shaped crack in a mesh for the uncracked structure in a fully automatic way. A subsequent finite element calculation determines the stresses ahead of the crack. These stresses are processed by CRACKTRACER to determine the (possibly mixed-mode) stress intensity factor distribution along the crack front. Using a user-defined crack propagation law, a crack increment is calculated and the procedure restarts with the new crack front, Fig. 27.

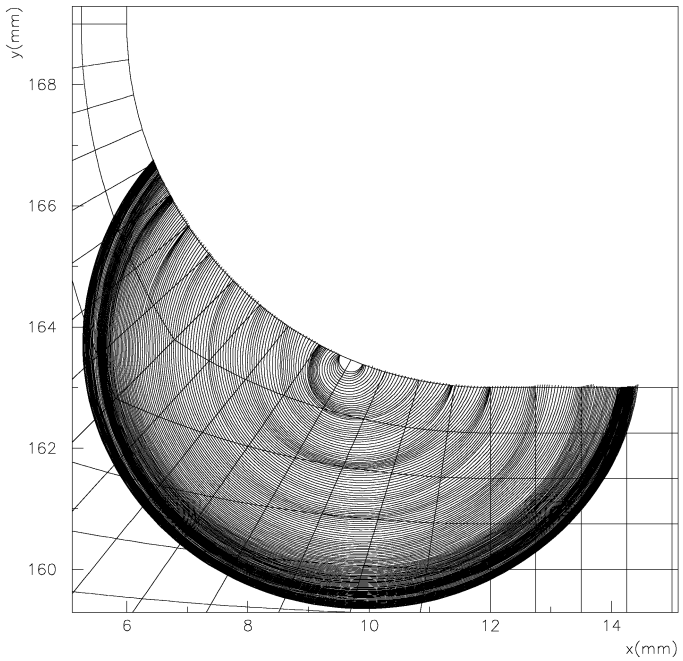

Fig. 27: Crack shape during propagation of a half circular initial crack in a disk.

- The program CRACKTRACER was enhanced to include crack propagation calculations in anisotropic materials. To this end, the singular stress field at the crack tip was determined using the finite difference method. By comparing the stress calculated by the finite element method with this asymptotic stress field, the K-factors are determined.
- A project is scheduled to investigate appropriate crack propagation laws for anisotropic materials. Different models will be included in CRACKTRACER and used to forecast crack propagation in Single Crystal test specimens. Experimental data are available, and show that the crack propagation depends on the orientation of the crack front with respect to the crystal. By comparing the experimental results with the predictions of CRACKTRACER, the parameters in the crack propagation laws will be determined.
- A new project was started to enhance the mixed-mode out-of-plane crack propagation capabilities of CRACKTRACER by including a so-called hex-tet mixed approach: for a given crack geometry a linear elastic calculation is performed with an automatically generated tetrahedral mesh. Then, the displacements in this mesh are used as boundary conditions for a local hexahedral mesh with collapsed quarter point elements at the crack tip (submodelling).

4.4 TMF Life Prediction Considering the Effective Damage Mechanisms

V. Bauer, H.-J. Christ, USI

In the field of jet engines, gas turbines, power and chemical plants, structural components working at high temperature under cyclic loading conditions are exposed to complex me-chanical and thermal load interactions. These interactions occur for example as a result of start-up and shutdown processes and are often the lifetime limiting factor for strongly loaded components.

Thermo-mechanical fatigue (TMF), where loading conditions involve both thermal transients and mechanical strain cycles, in the low cycle range (104–105 cycles) is one of the damage factor to be considered in the design of high temperature equipment. Thus, thermo-mechanical fatigue received much attention in recent years. As a matter of course TMF tests are not cheap also they are time-consuming. To meet the very severe requirements in design procedures (safety, reliability, efficiency, economy, etc.), it is reasonable to develop sophisticated lifetime predictions techniques, which take into account fatigue and creep behaviour as well as environmental degradation.

The objective of the underlying project is to investigate how far isothermal test data can be used to model tests under thermomechanical fatigue conditions and furthermore to find out where these tests show limitations to describe such

complex conditions (i.e., when a strong interdependency between the relevant damage mechanisms under TMF can be found).

For the high-temperature titanium alloy IMI 834, that has a target operating temperature of 600°C, a micro-crack propagation model was developed to predict thermo-mechanical fatigue life. Pure fatigue damage, which is assumed to evolve independent of time, is described using the cyclic J integral. For test temperatures exceeding about 600°C, oxygen-induced embrittlement of the material ahead of the advancing crack tip is the dominating environmental effect, whereas at intermediate temperatures hydrogen embrittlement from water dominates. To model the contribution of these damage mechanisms to fatigue crack growth, extensive use of metallographic measurements was made. Fig. 28 shows the results of the life prediction method developed. The curve labeled A represents the model prediction for tests con-ducted in a dry air, i.e., only pure fatigue and oxygen-enhanced fatigue crack growth are ac-counted for. Curve B gives calculated fatigue lives in a humid argon environment where hydrogen effects are important. Model prediction and experiments are in excellent agreement if pure fatigue damage and both environmental effects are included in the model, cf., curve C.

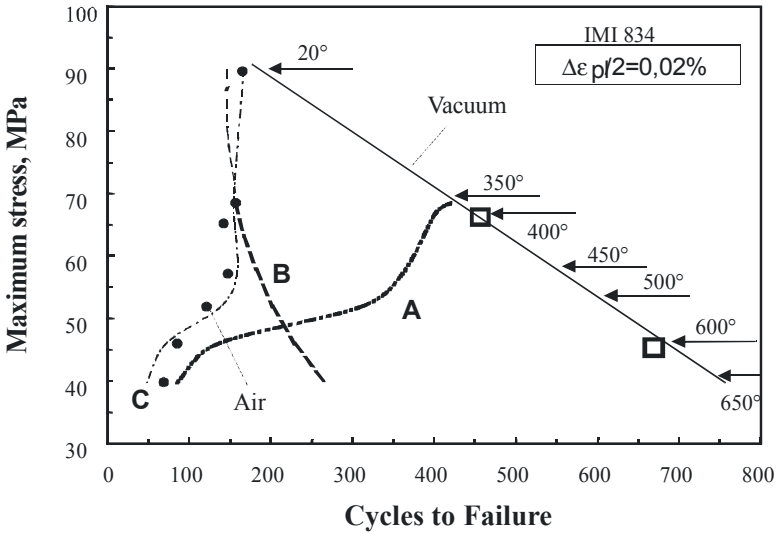

Fig. 28: Life prediction results on IMI 834 for isothermal loading conditions. Curves labelled A to C show various model predictions

5 FATIGUE AND FRACTURE OF METALLIC FUSELAGE MATERIALS

5.1 Service Load Tests on the Aluminium Alloy 2024

G. Kierner, UST-ISD

Service load tests for one of the most common aluminium alloys in light weight construction, alloy 2024, were carried out and the influence of strong mean load fluctuations for various period forms and period lengths was investigated.

a) Effect of load Spectrum Shapes on Program Fatigue Life

Three load spectrum shapes were investigated:

- Load spectrum shape of the Gaussian type
- Straight- line distribution
- Gust load spectrum

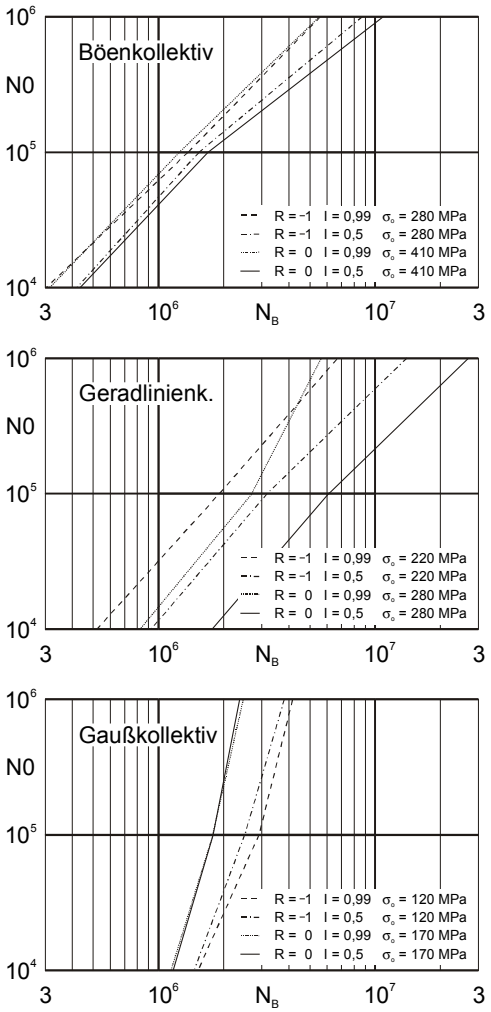

Fig. 29: Influence of the period length N0 and the regularity I on the life cycle N_B of 2024-T3 specimens (top: gust spectrum, middle: straight line distr., bottom: Gaussian spectrum).

b) Influence of the Period Length

Service load tests are normally carried out using a data set resulting from service measurements. These data generally represent a relatively small sample of the total of all loads a component has to bear during its life cycle. Laboratoty tests using this sample can lead to considerable faults in the evaluation of the life cycle of components unless corrections according to the sample size are also carried out.

The influence of the sample size was calculated on this basis of load changes with period lengths of 10^4, 10^5 and 10^6.

c) Influence of Regularity

The Regularity I represents the extent of the mean stress fluctuations of a load cycle and is defined as the quotient of the unidirectional mean load crossings N0 and the maxima respectively minima N1.

All service load tests were carried out for the regularity I = 0,99 (narrow band) and I = 0,5 (broad band).

d) Results

The figure shows the influence of the period length N0 and the regularity I on the life cycle N_B of the Gaussian type, the straight- line and gust load spectrum respectively for Al- alloy 2024 and form factor K_T = 3,6.

Since the S- N- curves are parallel for all distributions, any load level can be used for N0 across N_B; in the figure the lower level was chosen.

As can be seen from the double- logarithmic representation, the life cycle increases almost linearly with growing period length.

Whilst for the Gaussian type load spectrum the fatigue life values for I = 0,99 and I = 0,5 are nearly identical, they increase considerably for the gust load spectrum as well as for the strait- line spectrum.

5.2 Material Dependence of Long Fatigue Crack Growth in Thin Sheet Aluminium Alloys and Effect of Environment

F. Bergner, H. Bersch, K. Nocke, H. Worch, G. Zouhar, TUD-IfWW

The fatigue crack growth behaviour in the Paris regime of a number of thin sheet (thickness 1.6 to 2.5 mm) wrought aluminium alloys of different orientations (L-T and T-L) and aging conditions (T3, T4, T6, T7, T8) has been investigated by means of constant amplitude fatigue crack growth tests (sinusoidal waveform, R=0.1, σ_{max}=110 MPa, f=20 Hz, laboratory air). It has been shown that the materials can be subdivided into two groups. For the first group including the artificially aged conditions (but not the Al-Li alloys) the log(da/dN)-log(ΔK) curves strongly focus in a point at ΔK=10 MPa $m^{1/2}$. Furthermore, there is a rather strong correlation between the Paris exponent and a dimensionless material parameter composed of the 0.2% proof stress, the athermal strengthening coefficient, thickness, and the critical stress intensity factor for unstable crack growth [8]. For the second group including the naturally aged aluminium alloys and the Al-Li alloys the crack growth rate at ΔK=10 MPa $m^{1/2}$ is always less than for the first group and is correlated with the fracture surface roughness. The reasons for these types of behaviour have been analyzed. The material dependence of the environmentally assisted fatigue crack growth (3.5% NaCl solution) has also been investigated [9]. In Fig. 30 the frequency dependence of the environmental effect on fatigue crack growth is shown for alloy 6013 T6. The understanding of the mechanism of environmental influence and the identification of the rate-controlling steps are in progress.

5.3 Influence of Overloads on the Fatigue Crack Propagation in 7075T7351

M. Broll, S. Rödling, J. Bär and H.-J. Gudladt, UniBw-M

The knowledge of the influence of overloads on the fatigue crack propagation is very important for life time predictions of random loaded structural components. Corresponding tests to investigate the influence of overloads on the fatigue crack propagation under K-controlled conditions on SEN-specimens of a 7075 T 7351 alloy have been performed. The actual crack length was measured by a DC potential drop method and the load was calculated for the individual crack length to obtain a constant K-value. Finally, tests were undertaken with K_{max} as well as ΔK =const. In tests without any overload da/dN was constant (equilibrium). Differences in da/dN-values from this equilibrium condition, caused by a single overload, can be directly measured during the test with an extremely high resolution.

Fig. 31 shows the relative increase and decrease of the crack propagation rate da/dN caused by a 200 % overload (load increased by adding 200% of the normal K-value) as a function of the crack extension Δa. After a single overload the crack propagation rate increases up to 30 times of the equilibrium value. During this period the crack propagates only a few µm. The acceleration phase is followed by a retardation phase where the crack propagation rate decreases to about 8 % of the equilibrium value. The initial crack propagation rate da/dN =100% is reached after about 500 µm (point 2).

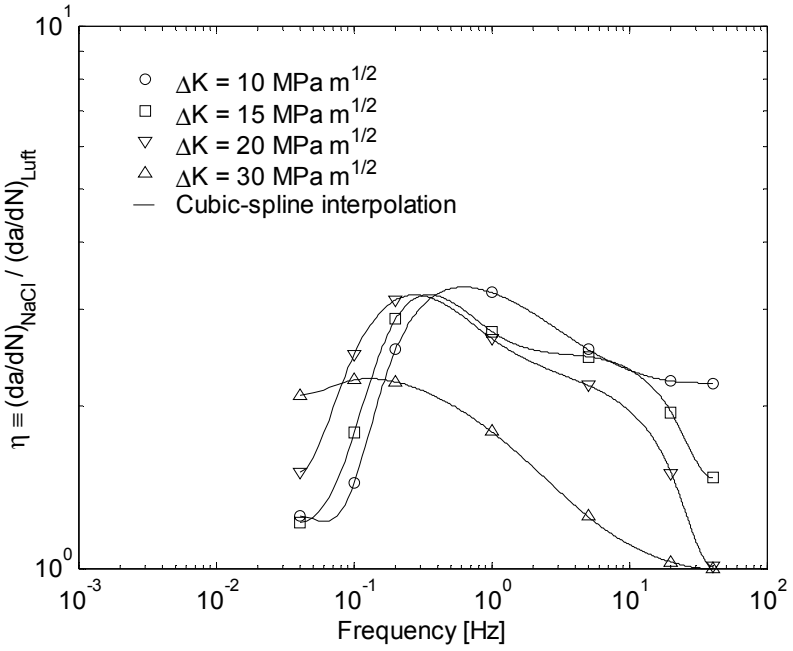

Fig. 30: Effect of frequency on environmentally assisted fatigue crack growth in 6013 T6 T-L (η: ratio of da/dN in NaCl to air).

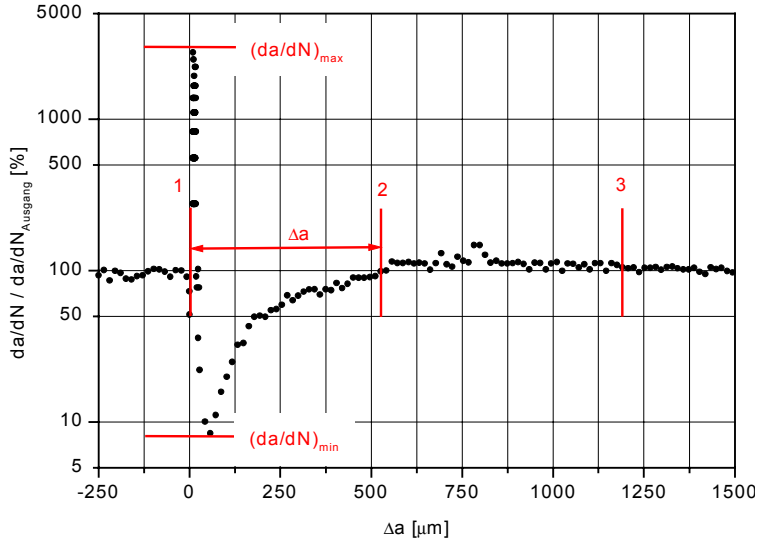

Fig. 31: Regions of increased and decreased crack propagation rates after a single overload.

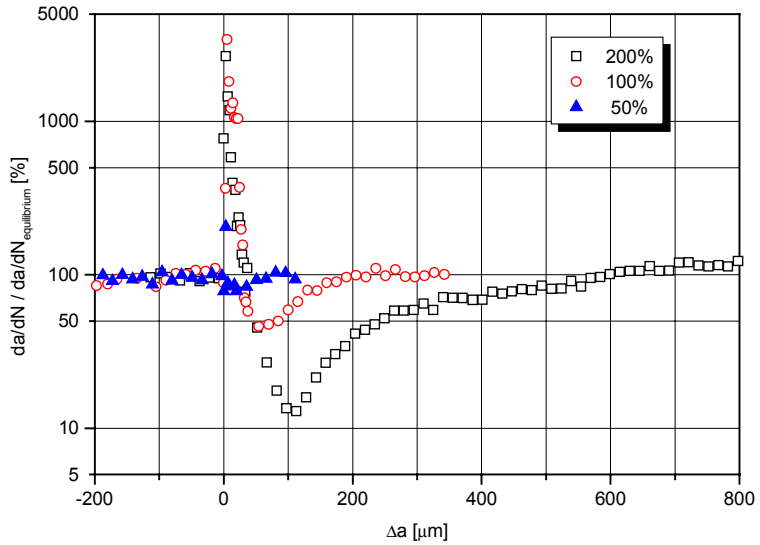

Fig. 32: Effect of the overload level on the influenced zone.

Thereafter, a broad region with an extension of about 1100 µm with slowly increasing crack propagation rate follows (point 2 – 3). Finally, the equilibrium value da/dN = const is reached behind point 3.

The amount of crack retardation and the extension of the area where the crack propagation rate is influenced by the overload sensitively depends on its maximum stress (Fig. 32). The extension of this area is about 50 µm, 200 µm and 600 µm in case of an 50 %, 100 % and 200 % overload, respectively. In addition, the amount of acceleration and deceleration of the crack propagation rate rises with the maximum stress of an overload. The decrease is very small for an 50 % overload, whereas, in case of an 200 % overload the crack propagation rate decreases to about 10 % of the start value. After an 400 % overload even crack arrest could be observed.

The observed behaviour can be explained by the formation of internal (residual) stresses in front of the crack tip. The formation of these stresses is caused by the overload. Our FEM calculations undertaken for the overload experiments showed a compression stress field followed by a tension stress field in front of the crack tip after a single overload. X-ray stress measurements by Jägg [10] undertaken on CT-specimens of steel lead to the same result. These internal stresses have to been added to the external stresses. Therefore, internal tensile stresses enhance the effective stresses in the crack tip region, leading to an increase of the crack propagation rate. Compression stresses however have to be subtracted from the external stress and, therefore, a decrease of the crack propagation rate has to be expected, as it has been found in our experiments.

5.4 Investigation about the Effect of Casting Surface Porosity on the Fatigue Life of A357-T6 Material

H. Moskopp, EADS-Airbus-H

During the manufacturing process it was notified that about 15% of all produced castings had a high surface porosity, which exceeded the acceptable levels. Since the influence of this porosity on the fatigue life was not known, it was decided to test coupons with this surface porosity.

The coupons were manufactured from a production casting with porosity. The coupon locations were specified to capture the worst areas of indicated porosity (with the most porous areas in the centers of the coupons).

Before cutting/machining the test bars, the casting was annealed and solution heat treated. At this point, the test bar areas were cut/machined from the casting and straightened. Machining of the coupons was done on three sides only, leaving the high porosity surface on one side (3 additional specimens were machined smooth on all sides to be used as control specimens). The coupons were then precipitation heat treated.

For the test two load cells were used, to increase the accuracy of low level loads: one calibrated at 5000 lbs full scale and a second one calibrated at 3000 lbs full scale. The machine allowed test frequencies between 3 Hertz (alternating stress of 120 MPa) and 10 Hertz (alternating stress of 60 MPa).

All in all, 3 smooth coupons and 9 coupons with surface porosity have been tested in fatigue at different load levels. The results of the smooth coupon tests were within acceptable limits of scatter for the basic A357-T6 material. The coupons with surface porosity showed a decrease in fatigue life, see Fig. 33.

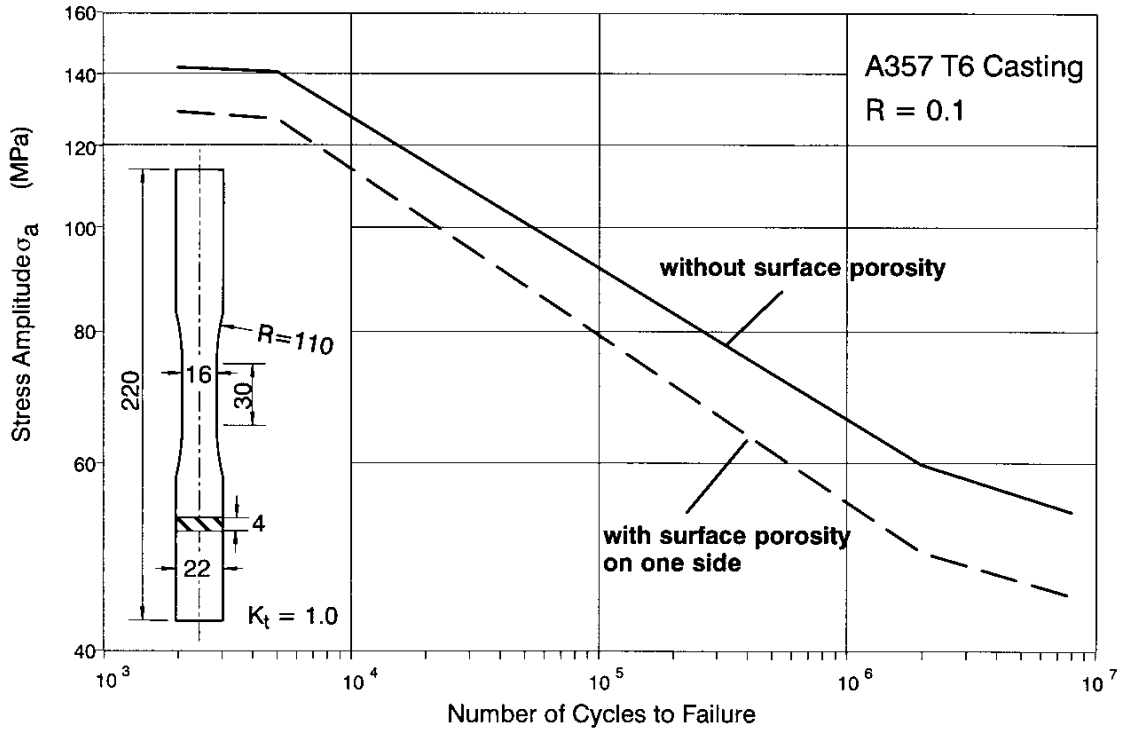

Fig. 33: Effect of High Surface Porosity on the Fatigue Life of the Al-Casting A357 T6.

5.5 The Fatigue Behaviour and Damage Mechanisms of Aluminium Foams

A. Ohrndorf, U. Krupp, H.-J. Christ, USI

Since the processing of aluminium foams has been improved in recent years, the homogeneity of the structure and the suitable mechanical properties of commercially available foams now lead to interesting applications especially in automotive and aerospace industries. Aluminium foams offer an enormous energy absorption capacity for passenger protection in crash accident in cars or planes. Their high stiffness associated with low masses is related to applications in lightweight structures such as bending-stiff surface structures of huge dimensions. Furthermore, aluminium foams provide improved passenger comfort using their heat- and noise-protective properties.

In this ongoing study two different aluminium foams are investigated. One was produced following the melt-route by introducing air into the molten aluminium building bubbles on the top surface which are stabilised by finely-dispersed SiC-particles added to the aluminium melt. In a continuous process the solidifying foam is skimmed from the melt by a conveyor belt yielding a stretched shape of the closed pores and a density of ρ=0,3 g/cm^3. The other foam was an open-cell foam with a density of ρ=0,15 g/cm^3 manufactured in a precision cast technique and reproduces a very homogeneous polymer foam.

For the comprehension of the fatigue behaviour of foams at first compressive and tensile tests were performed on simple rectangular specimens. In nearly static compression both materials show stress-strain-curves with an expanded region of constant stress ranging up to about 50% total strain, until global densification associated with disproportionate increasing stress sets in. The area beneath the stress strain curve represents the energy absorbed by the foam. In the region of constant stress damage occurs by the formation and the propagation of bands in which the deformation concentrates, whereas other parts of the specimen keep totally undeformed. In contrast to this, homogeneous deformation of the whole

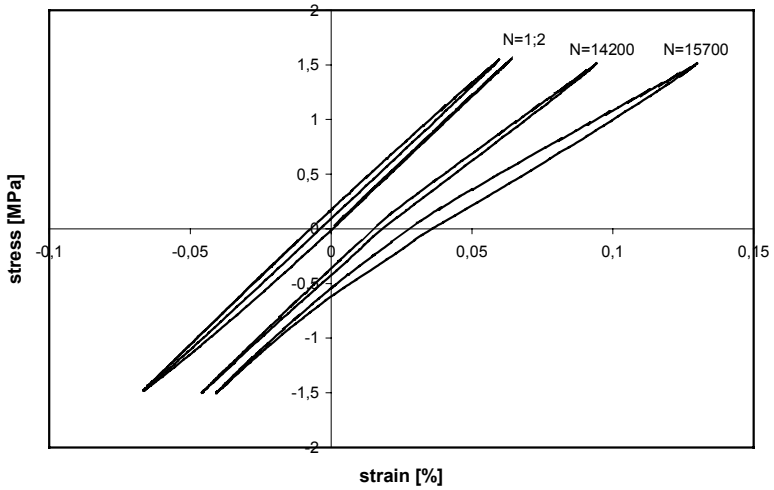

Fig. 34: Hysteresis loops of a fatigue test of a closed-cell aluminium foam.

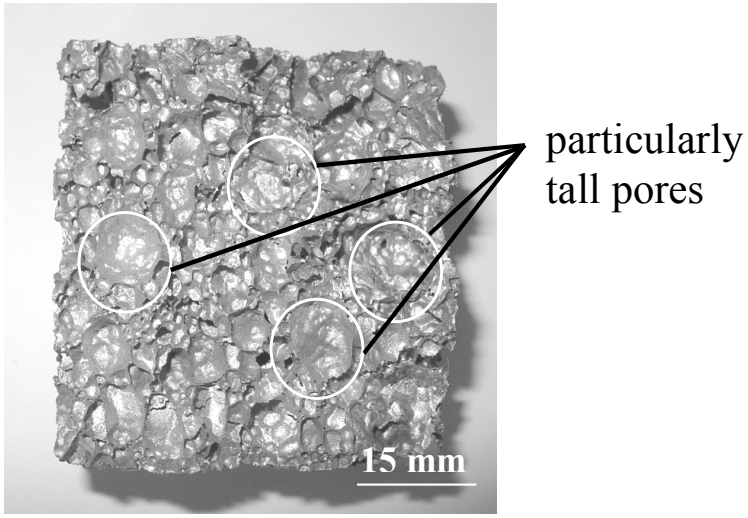

Fig. 35: Fracture surface of a fatigue specimen containing large pores.

specimen takes place in tensile tests ending in brittle fracture at a maximum strain of about 1%.

The detrimental influence of tensile stresses on the foam structure also becomes evident in fatigue tests performed under symmetric push-pull loads (R=-1) and sinusoidal wave shape. The progression of the hysteresis loops depicted in Fig. 34 suggest a kind of cyclic creep of the closed-cell foam. The formation of one single deformation band leads to a considerably increasing mean strain with increasing number of test cycles.

Not only cyclic creep but also fatigue crack propagation appears to be effective as a damage mechanism for the closed-cell foam which can be seen from the last hysteresis loop (N=15700) recorded close to the fracture of the specimen. According to the propagation of a fatigue crack the compliance increases in the regime of tensile stresses due to the missing contribution on the stiffness of the cracked parts of the specimen. In compression the cracked cell walls get in contact again resulting in a constant stiffness in compression.

The fracture surface of a fatigue specimen depicted in Fig. 34 shows a remarkable amount of pores with diameters of more than 10 mm which noticeably exceeds the average pore dimensions of the foam structure. Furthermore the cell walls found on the fracture surface tend to be quite thin and contain many cracked SiC-particles. Obviously the fatigue crack propagates through a cross-section featuring particularly low local density. The cracking of various particles also indicates high local stresses in the cell walls in the region of fatigue crack propagation. As SEM studies additionally showed the existence of striations on the fatigued cell walls a combination of cyclic creep and fatigue crack propagation can be considered as the relevant damage mechanism for cyclic loading conditions.

6 FATIGUE AND FRACTURE OF COMPOSITES

6.1 Damage Growth Investigations on Modern Carbon-Fibre Reinforced Composites

D. Paulisch, WIWEB, G. Loriot, CEAT France, H. Franz EADS Munich and A. Vinet EADS-CRC France

Damages to A/C-structures may occur at many occasions during an A/C life. It may happen during handling (i.e. falling tools), rolling (i.e. stones) and during flight (i.e. bird-strike). In metallic structures damages can easily be identified and assessed by dents or flaws on the surface. In composite structures those damages may only be barely visible and may be inside the material to quite an extend, such as hidden cracks or delaminations. With regard to the remaining life and residual strength of structural components it is therefore important to know, which degradation effects have to be expected. Furthermore, if any accidents may occur, it is important to be able to investigate and to judge, whether or not it was due to an immediate incident or impact, or the result of fatigue loading.

Thus, damage formation, damage detection, damage propagation and their effects on the performance of components made from carbon-fibre reinforced composites are more than ever a crucial point in the development of modern aircraft structures. In laboratory tests damages were therefore generated (impact-test), measured (ultrasonic measurements) and stimulated to propagate (fatigue-tests; acoustic emission and US measurements) in order to investigate the resultant losses of performance (static strength; fatigue) and to enable the evaluation of the causes of damage (SEM-investigations). The investigations are in progress.

A variety of nine different composite-materials of the following six configurations are/have been investigated at room temperature (23°C/50%r.h.), at increased temperatures (70°C/90°C) and in hot-wet climate (70°C/85%r.h.).

The number of materials of each type is marked in brackets. They are all potential candidates for structural materials for A/C-applications. The size of the test coupons was 150mm x 100mm x 4mm, according to the appropriate test procedure AITM 1.0010, Fig. 36:

- multidirectional prepreg-technique (epoxy (2); polyimide (1); thermoplastic (1))
- two-dimensional reinforcement with fabric-layers in prepreg-technique (1)
- two-dimensional reinforcement with fabric-layers in RTM-technique (1)
- two-dimensional non-crimp reinforcement with stitching in RTM-technique (1)
- two-dimensional fabric reinforcement with fixing in RTM-technique (1)
- three-dimensional woven reinforced in RTM-technique (1)

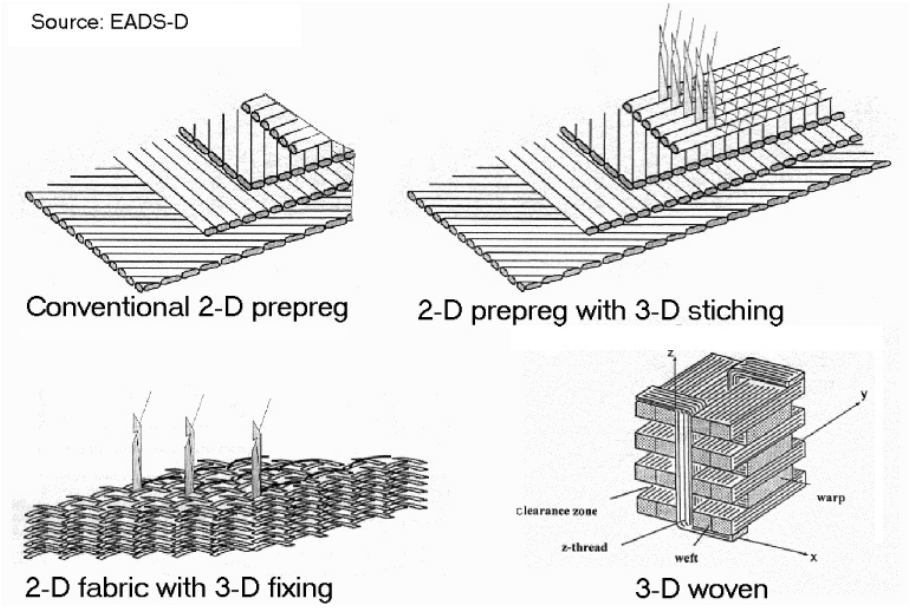

Fig. 36: Configurations of composites.

7 FATIGUE AND FRACTURE OF ENGINE MATERIALS

7.1 Fatigue of SiC-Fibre Reinforced Timetal 834 at Room Temperature and 600° C

P.W.M. Peters and J. Hemptenmacher, DLR-WF, H. Assler EADS-Airbus-H

SiC-fibre reinforced titanium is a candidate material for gas turbine components with a service temperature T<550° C, depending on the titanium alloy used. This material is produced at the Institute of Materials Research of the German Aerospace Centre (DLR) in Köln by coating SiC-fibres (SCS-6 fibres of Textron USA) with the titanium alloy by magnetron sputtering. Coated fibres are stacked in a preform after which consolidation takes part by HIPping at a high temperature and pressure (usually at 930°C and 190MPa for 30min). Fatigue behaviour at room temperature and 600° C has been investigated [11, 12] for the system SCS-6 / Timetal 834. Investigations are concentrated on the low cycle fatigue behaviour, so that the experiments are performed at a low frequency (f = 0.1 Hz up to 10^5 cycles, followed by f = 1 Hz up to 10^6 cycles and f = 10 Hz up to $5x10^6$ cycles). Results at room temperature, presented in Fig. 37, indicate the Wöhler curve can be divided into four ranges differing in dominating failure mode. Starting with the range with the lowest number of cycles up to failure the dominating failure mechanisms are:

range I: fibre failure

range II: fibre failure + matrix crack formation

range III: matrix crack formation bridged by unbroken fibres

range IV: at stresses at and below the endurance limit (matrix cracks are formed but are not able to break the fibres).

In Fig. 37 the different ranges for SCS6/Timetal 834 tested at room temperature are indicated. The borders between the different ranges are chosen rather arbitrarily. An exception is the maximum stress for the beginning of range III, indicated by the symbol *,which is taken at a stress at which ≤ 0.5% of the fibres break during the first cycle. This stress is calculated on the basis of a one-dimensional stress analysis considering elastic-plastic deformation of the matrix and a two-parameter Weibull strength distribution of the SCS-6 fibres.

The most important damage mechanism is that of range III, i.e. matrix crack formation. These cracks are bridged by initially unbroken fibres. The insets in Fig. 37 show two fracture surfaces of specimens cycled in this range. After heat tinting the specimen the coloured fracture surfaces indicate a bridged matrix crack covering 9% and 95% of the specimen cross section (A_{rel}=0.09 and A_{rel}=0.95), respectively. It is evident that the bridging fibres tend to keep the matrix crack closed, principally releasing the matrix crack tip intensity factor. A crucial role in this phenomenon plays the fibre/matrix interface. A strong interface reduces the crack tip intensity factor most. This takes place on disadvantage of

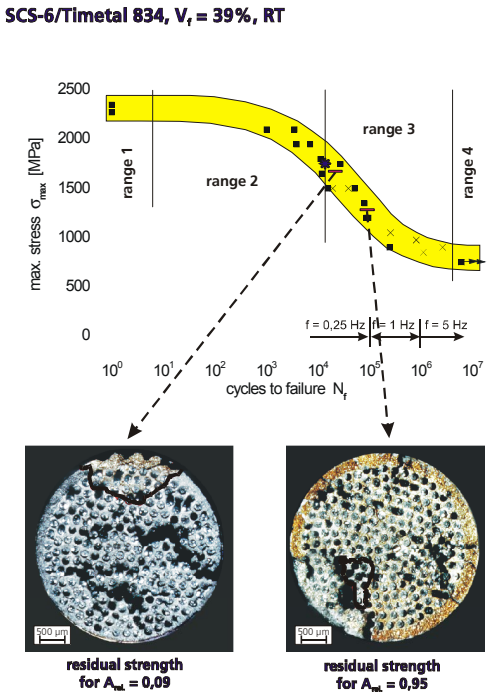

Fig. 37: Fatigue behaviour and fracture surfaces of SCS-6/Timetal 834 tested at 600°C.

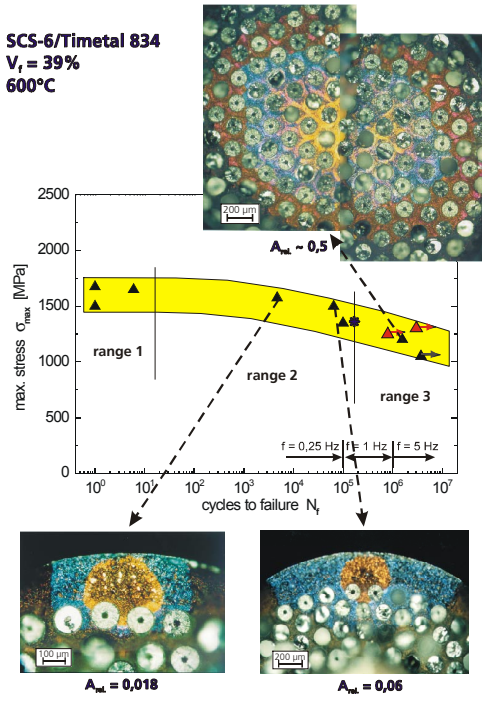

Fig. 38: Fatigue behaviour and fracture surfaces of SCS-6/Timetal 834 tested at 600°C.

the bridging fibres which could fail under the resulting overload. The poor to moderate fibre/matrix bond strength of SiC/titanium alloys proves to give the best fatigue strengths. Finite element calculations are performed to predict crack propagation rates for different conditions of interfacial stress transfer for the bridging fibres [13]. Assuming a negligible fibre/matrix bond strength and thus describing interfacial stress transfer only as a result of friction, it is found that the predicted crack growth rate (making use of the da/dN curves available for unreinforced Timetal 834) is larger than measured in SCS-6/Timetal 834 specimens. This shows the necessity to consider the fibre/matrix bond strength as well as frictional interfacial sliding to predict the crack growth rate in SCS-6/Timetal 834.

At 600° C the composite material proves to be less sensitive to matrix crack formation than at room temperature. Some of the specimens failed during 600° C testing due to matrix crack formation in the un-reinforced outer range of the specimens (see insets of Fig. 38). The two fracture surfaces shown indicate fatigue crack initiation in the transition zone between the area with sputtered matrix material and the titanium of the pre-form (here a tube of Timetal 834 into which a bundle of coated fibres is stacked). Only one specimen failed due to fatigue cracking starting from the specimen inside. The fracture surface of this specimen reveals matrix fatigue cracking over ~50% of the cross section. In contrast to the room temperature specimens which contained multiple matrix cracks, the 600°C specimens which survived the maximum number of cycles (2 to $5x10^6$ cycles) proved to contain hardly any matrix crack.. The main reason for the reduced sensitivity to matrix cracking and good fatigue behavior at 600° C is the stress relaxation of the matrix, which is efficient up to 10^5 cycles, as the frequency is only 0.1 Hz. Oxidation of the fibres at 600° C has been shown to severely degrade the fibres [14]. The present investigations, however, are not negatively influenced by oxidation, as the fibres are protected by the matrix. It is evident, that as soon as matrix cracks are formed at the surface bridging fibres suffer from oxidation. Thus it is likely, that the fatigue strength of the two specimens with the surface cracks covering 1.8% and 6% of the cross section of Fig. 38 (A_{rel}=0.018 and A_{rel}=0.06) are also influenced by oxidation of the fibres.

7.2 Fatigue of Ceramic Thermal Barrier Coatings for Gas Turbine Blades

M. Bartsch, B. Baufeld, K. Mull and C. Sick, DLR-WF

Ceramic thermal barrier coatings (TBC) with low thermal conductivity on internally cooled metallic turbine blades give a potential for increasing the gas inlet temperatures in a range of 50-150°C. Since, at higher gas inlet temperatures the remaining lifetime of the blade after failure of the TBC can be extremely short, reliable and practical lifetime assessment for TBCs is required.

Available testing methods only allow a ranking between different TBC-qualities with the uncertainty whether ranking under turbine engine service conditions will be the same as in simple tests. Therefore, a lifetime assessment concept based on realistic testing was developed [15]. The basic idea is to ensure that lifetime-limiting fatigue mechanisms during laboratory testing are the same as under service conditions including interaction effects between the different damaging mechanisms. A newly built thermal gradient mechanical fatigue (TGMF) testing facility, Fig. 39, allows simultaneous mechanical and thermal loading, including thermal shock. A thermal gradient is imposed by internal air cooling of the hollow cylindrical specimens [16]. The loading cycles during testing closely simulate the fatigue loads for a turbine blade in an aircraft engine during one flight. Since fatigue damages depend only on the number and amplitude of load alternations we reduced the time of one test cycle drastically to about one percent of a flight by diminishing the dwell times on certain load levels.

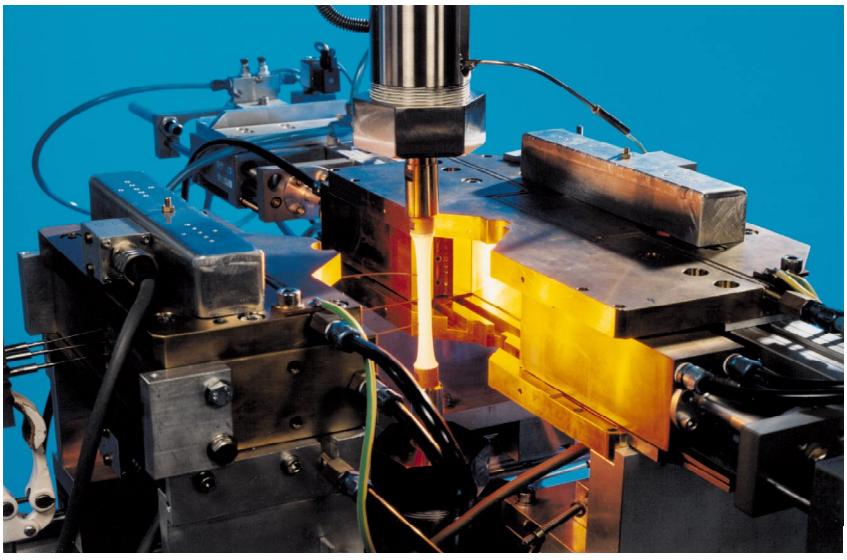

Fig. 39: Testing facility for thermal gradient mechanical fatigue (TGMF).

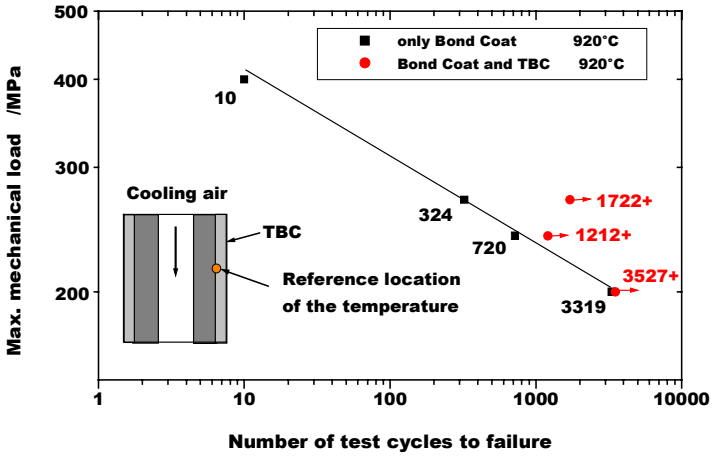

Fig. 40: Number of test cycles to failure. Lifetime of specimens without TBC can be describe by a power-law. All tests of specimens with TBC were terminated without failure of the TBC or the substrate.

Tests with electron beam – physically vapor deposited (EB-PVD) –TBCs revealed that the as-coated properties are sufficient to survive the required number of load alternations during service life [17], Fig. 40. Thus, the premature failure of TBC's observed in service implies the contribution of time-dependent damage mechanisms. In order to determine the interaction effects between fatigue and time-dependent damage mechanisms fatigue testing of pre-aged specimens will be conducted.

7.3 High-Temperature Fatigue Behaviour of an Intermetallic Gamma-Based Sheet Material

P. Schallow, H.-J. Christ, USI

Gamma titanium aluminides (γ-TiAl) are a class of intermetallic alloys that exhibit a great potential as high temperature structural material. As compared to Ni-based materials these alloys offer the possibility of substantial weight reduction, and in comparison to titanium alloys they possess better creep, oxidation and burn resistance, and increased strength at elevated temperatures. Applications identified as being interesting for γ-TiAl include gas turbine components like blades in the last stage of the low pressure turbine, as well as various other components such as high pressure compressor blades and vanes, casings, swirlers, diffusors, nozzle flaps and tiles, all examples from a jet engine.

While there are several studies which deal with the oxidation, creep and fatigue crack growth behaviour of TiAl-base alloys, only little information can be found on the high-temperature cyclic stress-strain behaviour. Especially, LCF testing of gamma-base intermetallic sheet-material is a fairly new research area and there is no published work on this topic to the authors' knowledge. The following results were obtained in the framework of a joint project (Brite Euram) with several industrial partners mainly from the aircraft industry. The overall aim of the project is the design and production of an exhaust cone made of a titanium aluminide sheet alloy.

Isothermal LCF tests were performed in air in total strain control under symmetrical push-pull conditions (R=-1) with a triangular wave shape of the command signal. In order to allow testing of the specimens (thickness from 1.5 down to 0.7 mm) at negative R-values the specimen needs to be supported by a special Anti-Buckling Device (ABD) to avoid Euler-buckling under compressive stresses. On the one hand the ABD should provide a close guide of the specimen, what is particularly important if the alloy behaves in a brittle way, on the other hand any effect on the test results, e.g. the fatigue life, as a consequence of friction should be avoided. The design of the ABD as shown in Fig. 41 was found to give satisfactory results.

Like many other gamma-base intermetallics, the alloy studied showed a distinct brittle to ductile transition (BDT) in its LCF behaviour at a temperature of approximately 650 °C which was also found in preceding tensile tests. Fig. 42 depicts plastic and total strain hysteresis loops taken from a LCF test carried out at 550 °C at a total strain range of 0.5 %. The lower part of the plastic hysteresis loop reveals a pronounced bending which is increased towards the load reversal point in compression. The apparently reduced stiffness at the load reversal point can be attributed to buckling-induced increase in compliance of the specimen under compressive load. At 550 °C, which is below the BDT-temperature, the cyclic deformation behaviour is characterized by cyclic hardening during cyclic loading. This transient process leads to

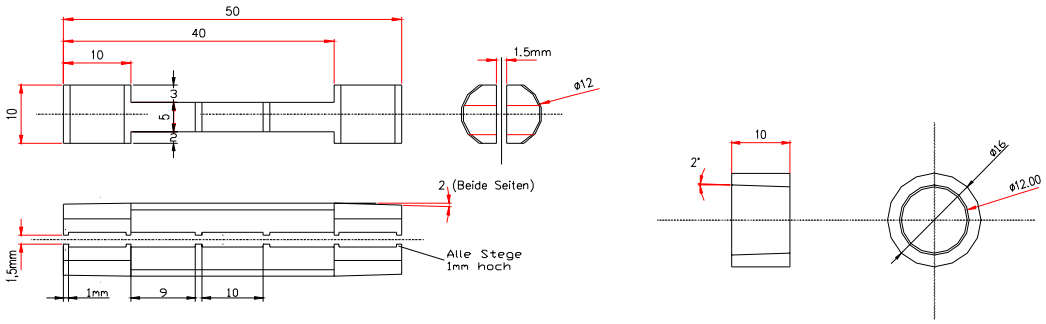

Fig. 41: Anti Buckling Device (ABD) designed for LCF testing of the intermetallic sheet material.

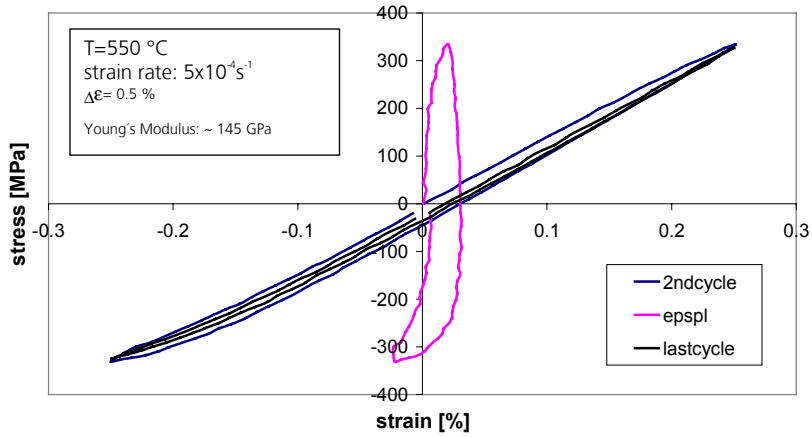

Fig. 42: Hysteresis loops of γ-TiAl intermetallic tested at 550 °C.

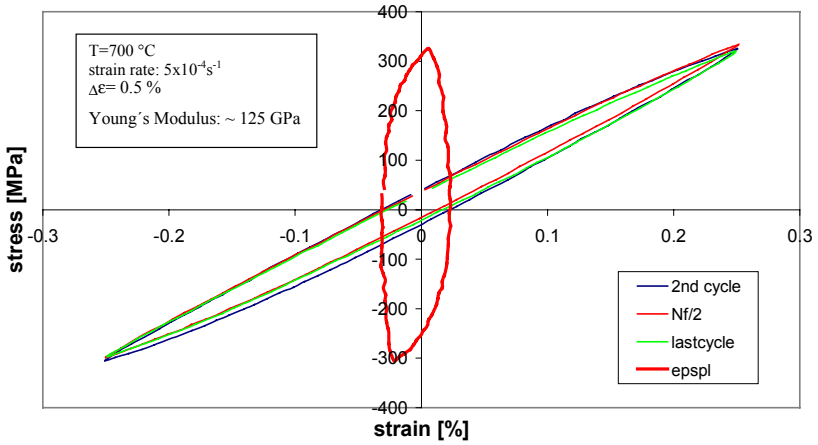

Fig. 43: Hysteresis loops of γ-TiAl intermetallic tested at 700 °C.

a change in the shape of the hysteresis loop. The total strain hysteresis loop taken from the last cycle shows a very narrow shape indicating a decrease in the plastic strain range.

Conversely, tests carried out above the BDT-temperature did not show cyclic hardening. Fig. 43 shows typical results of a test run at 700 °C under identical test conditions. The total strain hysteresis loops taken from the second and last cycle nearly retain their shape indicating a state of cyclic saturation. In contrast to the cyclic hardening observed below the BDT-temperature, this deformation behaviour above the BDT-temperature is beneficial with regard to fatigue life meaning that fatigue life increases with increasing temperature. Moreover, at elevated temperatures the effect of buckling becomes negligible which can be attributed to the increased plasticity above the BDT-temperature.

7.4 Thermohydrogen Processing (THP) of Metastable Beta Titanium Alloys

G.M. Lohse, A. Senemmar, K. Prüßner, H.-J. Christ, USI

Hydrogen is known to deteriorate the mechanical properties and lead to brittle fracture behaviour of most structural alloys. The uptake of hydrogen can taken place during production, surface treatment and in service under respective environmental conditions. As opposed to the embrittling effect of hydrogen, although a positive effect on the mechanical properties may result under certain conditions.

The object of this ongoing study is to investigate the effect of hydrogen on the microstructure and to characterize the variation of the mechanical properties in metastable ß titanium alloys by means of thermohydrogen processing. In the case of metastable ß-titanium alloys, hydrogen has strong influence on the microstructure, because hydrogen acts as an ß-stabilizing element. This provides the possibility to optimise the microstructure and final mechanical properties.

Two commercial titanium alloys are studied. The tested materials are the metastable ß-titanium alloys Timetal®LCB (low cost beta, Ti-6.8Mo-4.5Fe-1.5Al) and Timetal®10V-2Fe-3Al, which are charged by a two-step heat treatment to various hydrogen concentrations. The mechanical properties corresponding to these hydrogen-charged conditions are characterized in fatigue tests under total stain control, fatigue crack propagation tests, tensile tests and Charpy notch impact tests. It was observed that specimens of Ti 10V-2Fe-3Al, which were charged to various hydrogen levels by means of solution annealing at a temperature of 40°C below the ß-transus (810°C) for 2 h in helium/hydrogen gas mixtures, contain a reduced volume fraction of primary α - phase. For a content of 6 at-% hydrogen α-phase was completely absent. Therefore, subsequent aging at 500°C for 8 h led to two-phase microstructures consisting of bcc ß-matrix with needle-shaped α precipitates as shown in Fig. 45. In comparison, the hydrogen-free reference condition (H-content less than 0.2 at-% in the as-received condition) shows both primary α as isolated grains formed at triple points of the ß-matrix and the fine secondary α precipitates embedded in the ß grains (Fig. 44).

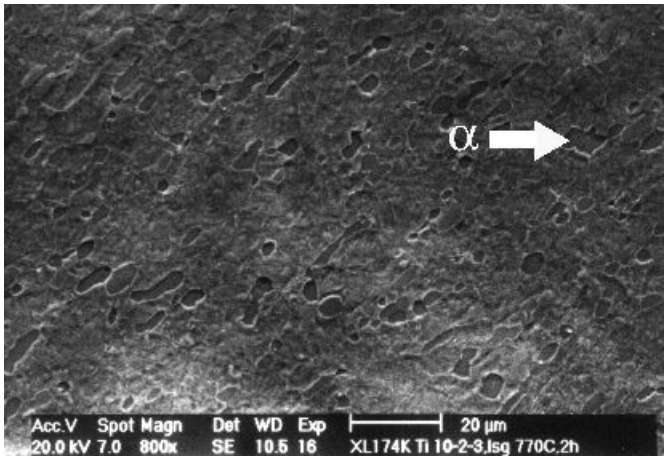

Fig. 44: SEM image showing the microstructure of Ti 10V-2Fe-3Al (primary α-phase) after solution-annealing and subsequently aging without hydrogen processing.

Fig.3 represents the cyclic deformation curves of Ti 10V-2Fe-3Al of various hydrogen concentrations resulting from the above described heat treatment. The test were performed at a total strain amplitude of $\Delta\varepsilon/2=1.2$. The results indicate that moderate hydrogen contents increases strength and decreases cyclic life under cyclic loading conditions. High hydrogen levels show increased numbers of cycles to failure as a consequence of a decrease in strength. This is due to the fact that the volume fraction of the particle-strengthening α-phase decreases with hydrogen content.

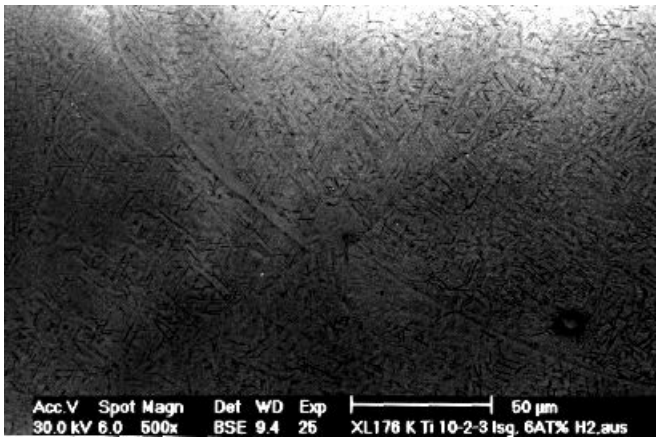

Fig. 45: SEM image showing the microstructure of Ti 10V-2Fe-3Al (secondary α-phase -phase) after solution-annealing in hydrogen environment up to a content of 6.07 at-% hydrogen and subsequently aging.

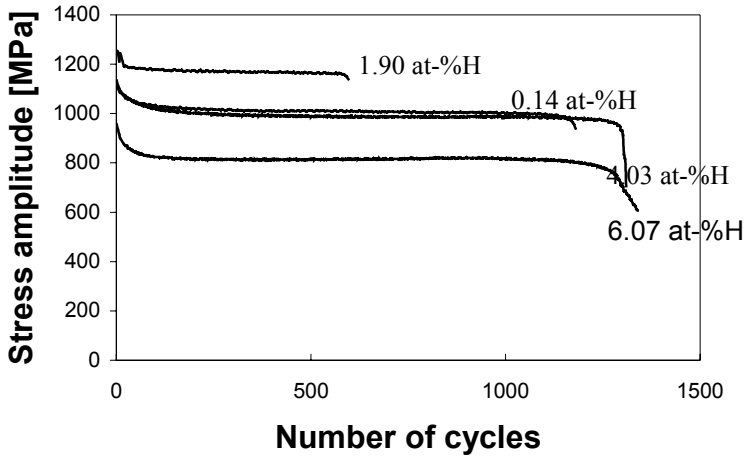

Fig. 46: Cyclic deformation curves of Ti-10V-2Fe-3Al solution annealed in He/H2 to different hydrogen concentrations and subsequently aged.

7.5 Initiation and Propagation of Microstructural Short Cracks in a Beta-Titanium Alloy

W. Floer, J. Lei, Y.M. Hu, U. Krupp, H.-J. Christ, A. Schick, C.-P. Fritzen, USI

The initiation and the early growth of fatigue cracks are strongly influenced by microstructural features like grain boundaries, grain size and the local crystallographic orientation. Even under an applied loading below the macroscopic yield strength some grains exhibit high mechanical stresses due to the anisotropy of the elastic properties particular in the vicinity of the grain boundaries. This was shown in the present study by fatigue tests on the beta-titanium alloy Timetal®LCB (low cost beta, Ti-6.8Mo-4.5Fe-1.5Al), which were periodically interrupted for examining the shallow-notched gauge length by scanning electron microscopy in combination with the EBSD technique (electron back-scattered diffraction) with regard to the occurrence of microstructural short cracks and the crystallographic orientation of those grains which participate in crack initiation processes. The results in combination with local displacement measurements during fatigue testing, which were carried out by means of an interferometric strain/displacement gauge (ISDG), allowed the calculation of the elastic anisotropy and the resulting stress distribution by applying the finite-element method (FEM) at the surface. As an example, Fig. 47 shows an intergranular short crack which obviously results from the high stresses which are caused by the elastic anisotropy as proved by FEM (Fig. 47b).

Besides the significance of the crystallographic orientation on crack initiation, also crack propagation was found to be strongly affected. The extent of crack retardation at grain boundaries was observed to depend strongly on the misorientation angle. Moreover, crack closure/opening effects seem to play an important role. For fully reversed loading and

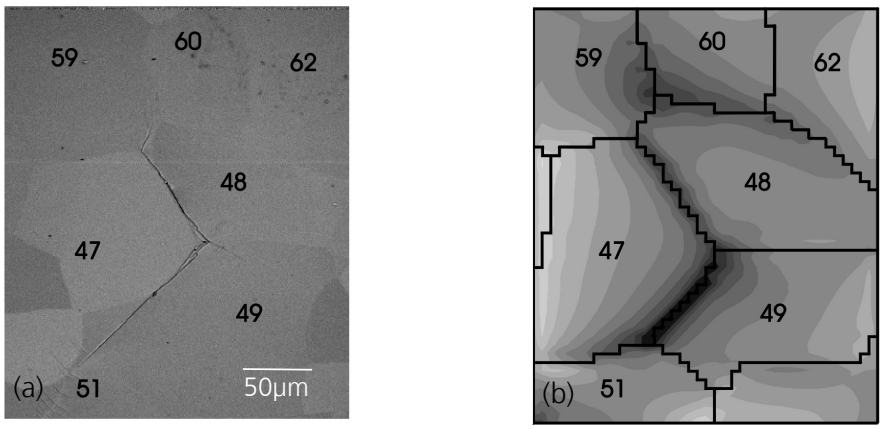

Fig. 47: Intergranular crack initiation: SEM micrograph (a) and corresponding calculated stress distribution (b) (maximum mean stresses: high stress values = dark) ($\Delta\sigma/2$=600MPa $\Leftrightarrow$)

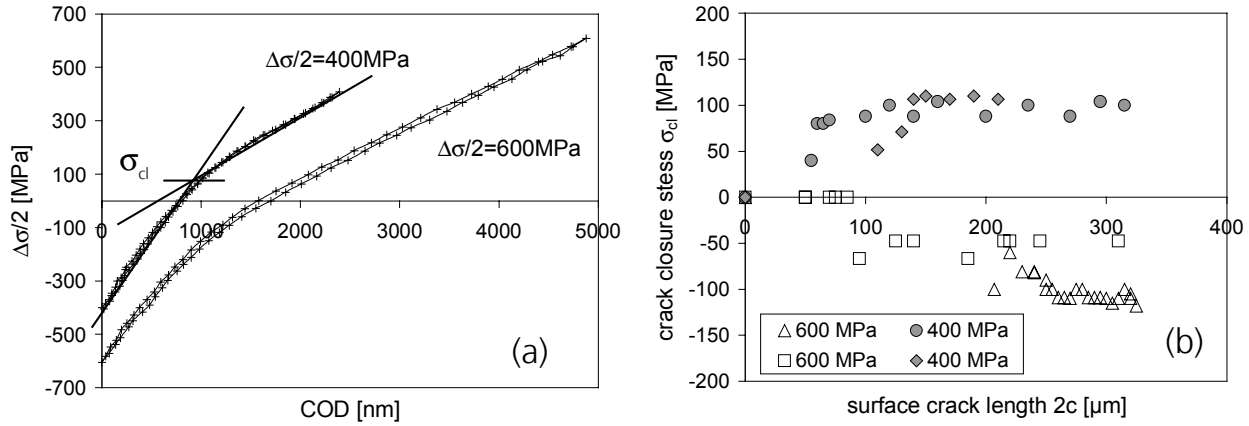

Fig. 48: Evaluation of crack closure effects: stress vs. crack opening displacement (a) and crack closure stress vs. crack length (b).

high applied stresses, cracks close in the compressive regime (Fig. 48). This behaviour is in contrast to the plasticity- and roughness-induced closure effects usually observed for long crack propagation, where a premature contact of the crack surfaces already happens under tensile stress and a respective strong decrease the crack driving force occurs.

In the ongoing study the observed interactions between microstructure and growing short cracks will be incorporated into a numerical computer simulation, which is based on the short crack growth model of *Navarro* and *de los Rios*. The final objective is to establish a mechanism-oriented life prediction concept for cyclically loaded components.

7.6 High-Temperature Fatigue Behaviour and Damage Mechanisms of the SiC-Reinforced and Dispersoid-Strengthened Aluminum Alloy X8019

A. Jung, H.-J. Christ, H.J. Maier, USI

Aluminium alloys which are discontinuously reinforced with SiC particles are very attractive materials for structural applications especially in aerospace industries due to their high strength and stiffness at low density. A detailed knowledge of the fatigue behaviour of this class of materials is an important prerequisite for a reliable and safe application as oscillating and rotating components. The useable temperature range can be extended to about 350°C, if the matrix of these alloys is strengthened by thermally stable dispersoids. Very limited information on those damage mechanisms exists which result from fatigue loading at high temperatures in dispersoid-strengthened and particle-reinforced aluminium alloys.

In order to characterise the effects arising from the existence of SiC particles, the dispersoid-strengthened high-temperature aluminium alloy X8019 (Al-8Fe-4Ce) and the same alloy reinforced with 12.5 vol. pct SiC particles (average diameter: 3µm) were studied comparatively. Both alloys were produced via a powder-metallurgy route from rapidly solidified gas-atomised powders. After solidification, both alloys are strengthened by thermally stable dispersoids of the same content and morphology.

Isothermal low cycle fatigue (LCF) and thermomechnical fatigue (TMF) tests were performed on smooth mechanically polished specimens. Symmetric push-pull true plastic strain control was applied using a triangular command signal. The temperature range under consideration was from room temperature to 350°C. TMF testing was conducted with the temperature either increasing (in-phase (IP) tests) or decreasing (out-of-phase (OP) tests) with increasing plastic strain. For lifetime prediction crack growth measurements using single edge notch bend (SENB) specimens loaded in 4-point bending and conventional tensile creep tests were carried out.

SEM study revealed a distinct change in damage mechanism both with increasing temperature under isothermal conditions and with testing mode of TMF loading (i.e., ε_{pl}-T phase shift). In isothermal tests at room temperature as well as in TMF OP tests, cyclic life is determined by fatigue crack growth which takes place mainly within the matrix. Cracked SiC particles were found only on the fracture surfaces, i.e. cracking occurs in the stress field of the propagating crack, while within the bulk (remote from the main crack) particles debond from the matrix and almost no cracked SiC particles exist. At elevated temperatures and under TMF IP conditions, voids are formed at the SiC/matrix interface as a bulk phenomenon, and cracking of particles in front of the growing crack seems to lose importance with increasing temperature. Thus, under these conditions fatigue cracks first extend preferentially within the matrix and later propagate by link-up with the SiC/matrix interface voids.

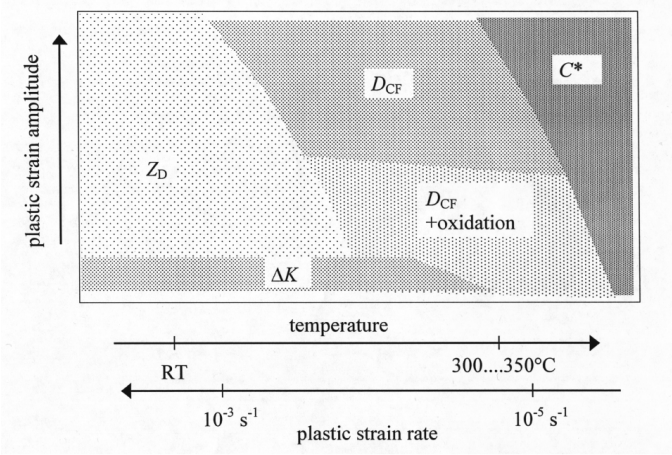

Fig. 49: Schematic map representing the regimes of the respective lifetime prediction method applied.

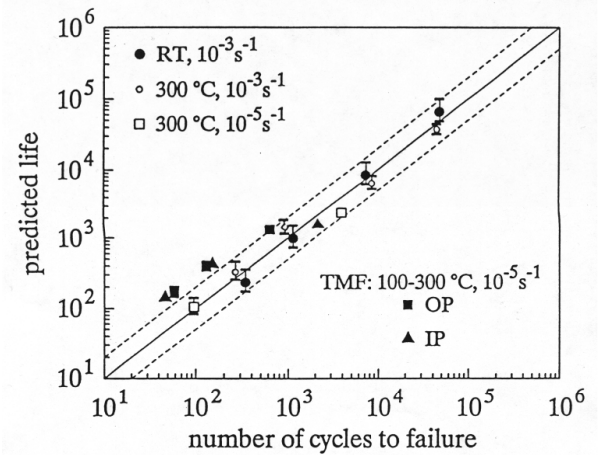

Fig. 50: Comparison of predicted and measured cyclic lives. Error bars shown refer to initial crack length scattering.

The knowledge of the respective relevant damage mechanism provides a sound basis to select the appropriate concept for lifetime prediction. In Fig. 49 the corresponding approaches offered by fracture mechanics are depicted. The description of fatigue crack growth by means of the cyclic stress intensity factor holds true as long as linear-elastic deformation prevails. Under the fully plastic deformation conditions of both the isothermal LCF and the TMF tests concepts of the elastic-plastic fracture mechanics can be applied. If fatigue life is determined by fatigue crack propagation, the cyclic J-integral, often called Z-integral, can be used. At temperatures above 250°C time-dependent plastic deformation, i.e. creep, has to be taken into account. For this purpose, Riedel [18] introduced the damage parameter D_{CF} for creep-fatigue based on a material law for elastic-viscoplastic solids.

In order to predict fatigue lifetime for TMF loading conditions, it was assumed that the overall fatigue crack growth rate can be assessed by a linear summation of terms resulting from pure fatigue and contributions from creep and oxidation. Since gas/metal interactions are known to show a very strong temperature dependence, the maximum temperature within a TMF cycle was considered to be decisive for the oxidation effect. A detailed description and discussion of the whole procedure applied is given in ref. [19].

Fig. 50 compares the experimentally observed fatigue lives with the results of the prediction for both the isothermal and the TMF tests. The dashed lines mark the range within which the deviation between prediction and actual value is better than a factor of 2. Generally, TMF loading led to a life reduction as compared to isothermal tests even if the behaviour at the maximum temperature of the TMF cycle is considered. The prediction accuracy of TMF life at higher plastic strain amplitudes is relatively poor and non-conservative values result. Under these loading conditions a strong coupling of damage mechanisms occurs in a way that is not reflected in isothermal tests. Hence, TMF lifetime prediction from isothermal data is hardly possible.

8 NON-DESTRUCTIVE TESTING

8.1 Structure Integrated Acousto-Ultrasonics and Related Signal Processing for Monitoring Cracks in Aluminium Plates

C. Boller, EADS-M, C. Biemans, DaimlerChrysler, Mercedes-Benz, Sindelfingen/Germany, W. Staszewski and G. Tomlinson, Dept. of Mech. Engineering, Univ. of Sheffield/UK

Acousto-ultrasonics is a method known in non-destructive testing, where an acoustic wave is sent through a component by a piezoelectric element working as an actuator and the wave is recorded by another piezoelectric element as a sensor. Such a method has been applied for monitoring crack propagation in simple aluminium panels as shown in Fig. 51. This 400x150x2 mm plate had a 1.5 mm crack which was initiated by spark erosion in the centre of the plate. The plate was fatigue loaded at 6 Hz with a load amplitude of ± 11.5 kN load amplitude and a mean load of 12.5 kN respectively. The plate was instrumented with 6 piezoceramic elements (PZT Sonox P5, 15x15x1 mm) fixed in a symmetrical configuration on both sides of the crack. For monitoring crack growth the acousto-ultrasonics method was used where the bottom right hand side piezoelectric element was used as an actuator. A Gaussian white noise with a maximum frequency of 25 kHz was used as an input signal.

The variance of the orthogonal wavelet coefficients was calculated for all wavelet levels representing data sets of two

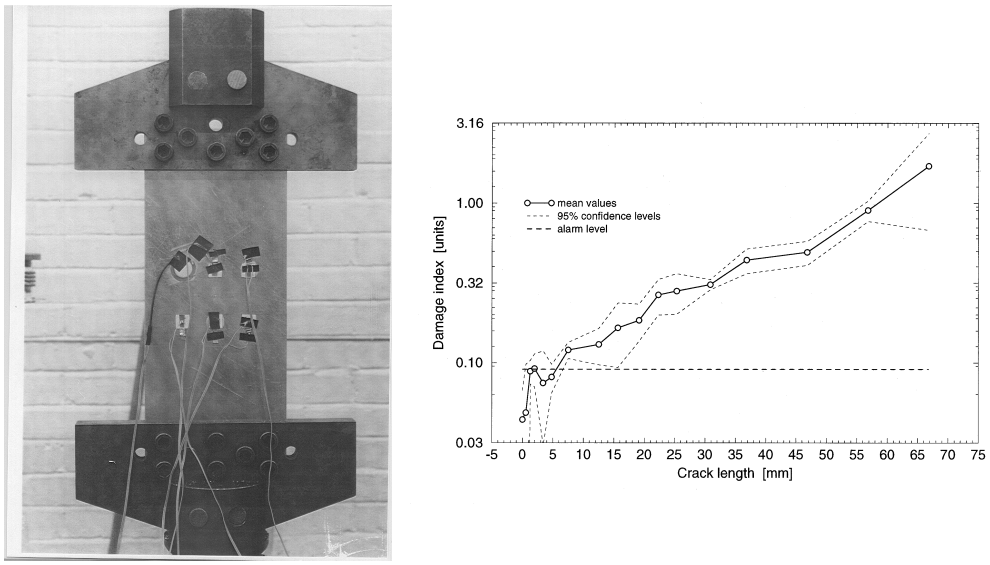

Fig. 51: Cracked aluminium plate and resulting wavelet based sensor signal evaluations.

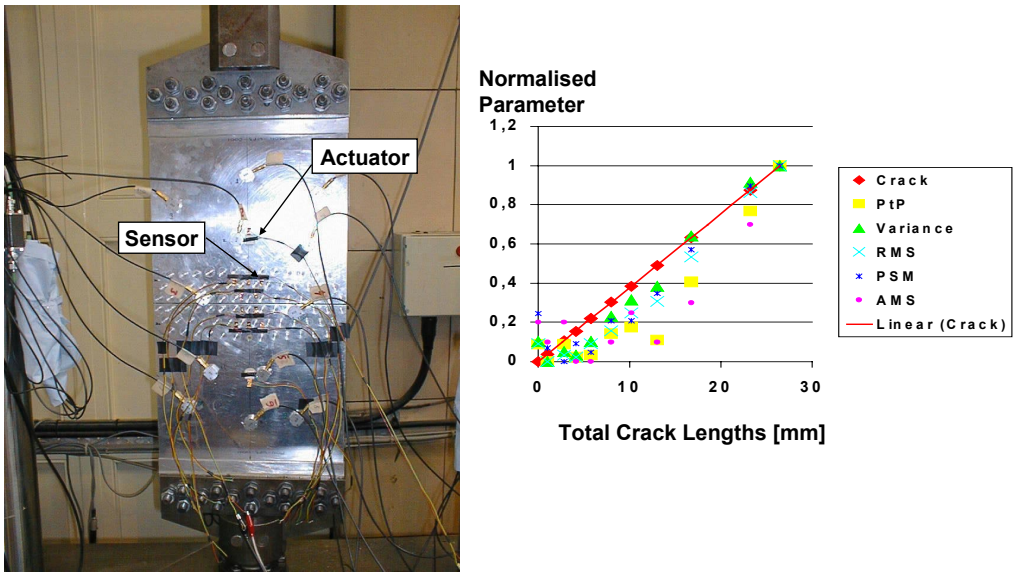

Fig. 52: Crack propagation monitoring in multi-riveted aluminium panel.

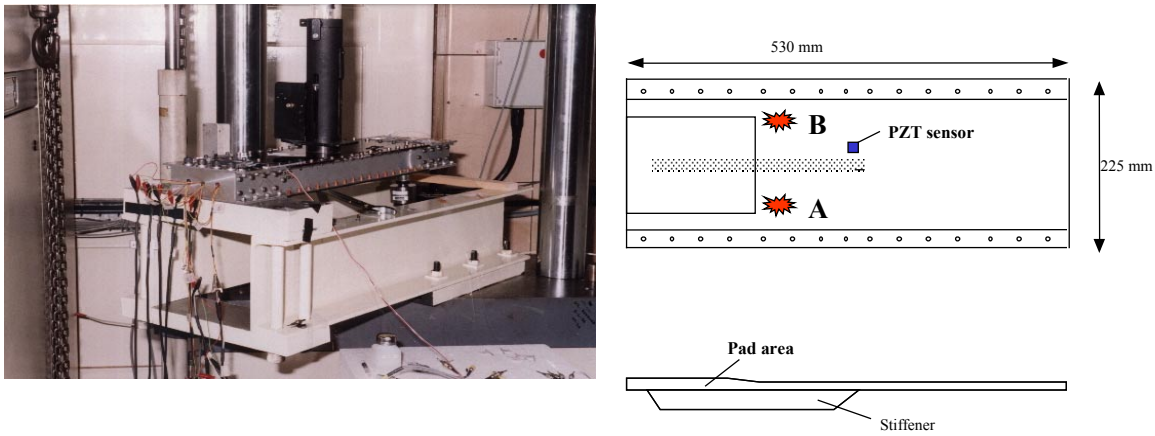

Fig. 53: Composite specimen with piezoelectric sensor

different sensors. The damage index was selected as the Euclidian distance between the mean vector of the logarithmic variance and the wavelet variance characteristics. The result of such an evaluation is shown in Fig. 51 as the logarithm of the damage index versus crack length. Here crack growth can be clearly seen for a crack growing from 6 mm onwards.

In another test a multi-riveted aluminium plate of 750x300 mm as shown in Fig. 52 was fatigue tested. Again the same type of piezoelectric element as mentioned above was placed as sensors between the rivet lines and as an actuator on the top, with the other sensors being classical acoustic emissions sensors used for benchmarking. The actuator input signal was now up to 500 kHz. Different parameters obtained from the time domain sensor signals have been evaluated, normalised and compared to the sum of crack lengths monitored visually, where the result is shown on Fig. 52. The closer the results follow the 45° line, the better the parameter considered which turned out to be best for the variance in the time domain signal.

8.2 Structure Integrated Acousto-Ultrasonics and Related Signal Processing For Monitoring Impact Damage in Composites

C. Boller, EADS-M, C. Biemans, DaimlerChrysler, Mercedes-Benz, Sindelfingen/Germany, W. Staszewski and G. Tomlinson, Dept. of Mech. Engineering, Univ. of Sheffield/UK

Acousto-ultrasonics is a method known in non-destructive testing, where an acoustic wave is sent through a component by a piezoelectric element working as an actuator and the wave is recorded by another piezoelectric element as a sensor. Such a technique has been applied for composite plates fabricated from carbon/epoxy T300/914 unidirectional prepreg which were mechanically fastened to a stiffening aluminium sub-frame and attached to a metal loading frame as shown in Fig. 53. A more detailed description of the test can be found in [20].

The piezoelectric elements were used to monitor impacting events. High-frequency strain data gathered were decomposed using the orthogonal wavelet transform. For the damaging impact energies at impact locations A and B clear spikes could be identified for the higher frequency wavelet decomposition. This spikiness of the data has been analysed using Kurtosis, which is a normalised 4th spectral moment [21]. Fig. 54 gives the values of Kurtosis for the analysed impact signals for position A at different impact energy levels. A difference between damaging and non-damaging impacts can be clearly identified. The values for Kurtosis were also determined for the original time domain data where no significant difference could be seen for the different impact loads.

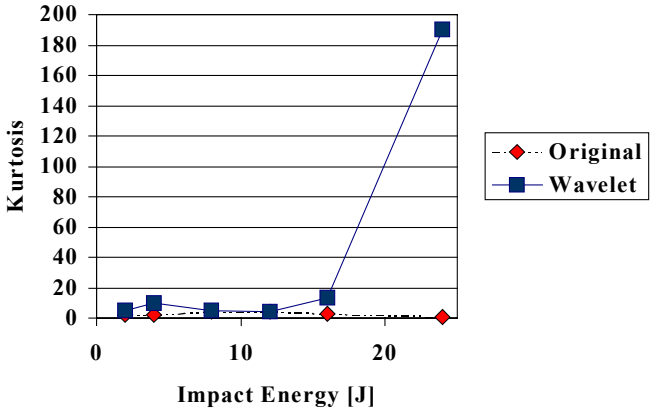

Fig. 54: Kurtosis characteristic for the impact strain data

9 INVESTIGATIONS OF GENERAL INTEREST

9.1 Lifetime Prediction in the High Cycle Regime

H. Zenner, S. Pöting and M. Traupe, TUC-IMAB

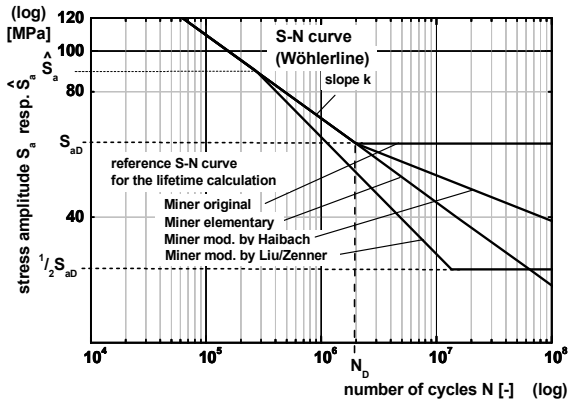

Fig. 55: Reference S-N curves for lifetime calculation using Miner-Rule modifications.

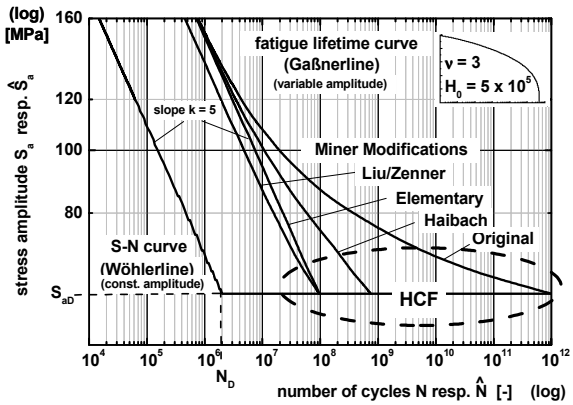

Fig. 56: Lifetime predictions using Miner-Rule modifications.

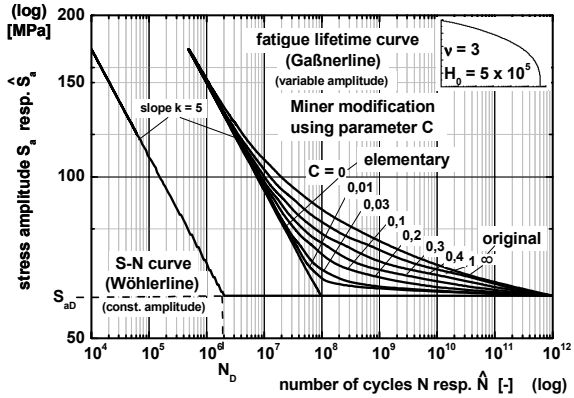

Fig. 57: Lifetime predictions using the C parameter.

Many components are subjected to variable amplitude loads and many of them are exposed up to 10^8 or even more load cycles during their utilization. Often failure occurs when the applied maximum stress value of the cumulative frequency distribution is just above the fatigue limit.

Lifetime predictions for components in the high cycle regime are still inadequate [22-24]. A main reason for the inadequacy is the insufficient knowledge about the damaging mechanisms and the lack of valid simulation models to describe the fatigue process.

Usually an analytical fatigue lifetime prediction is performed using the nominal stress concept and the Palmgren-Miner-Rule for the linear damage accumulation. A comparison of prediction and experiment shows a large uncertainty [22-24]. Miner-Rule modifications have been developed to improve the fatigue lifetime prediction [25]. None of the Miner-Rule modifications is capable to describe all test results. The modifications have a significant influence on the predicted fatigue lifetime especially in the high cycle regime when the maximum stress value is just above the fatigue limit. At a high maximum stress value all predictions by the Miner modifications except the modification by Liu/Zenner predict the same lifetime, Fig. 55 and Fig. 56.

The modifications of the Miner-Rule differ in the assumption of the contributed damage for stress amplitudes below the fatigue limit. Miner original assumes no damage for those amplitudes. Miner modified by Haibach assumes a fictitious reference S-N curve with a reduced slope. Miner elementary assumes a fictitious reference S-N curve prolonged below the fatigue limit. Miner modified by Liu/Zenner uses a steeper fictitious reference S-N curve for the damage accumulation. Based on experimental results Liu/Zenner define an assumed new lower limit at ½ SaD [26]. Another modification introduced in 1988 by M. Hück [27] suggests a decreasing slope of a reference S-N curve, Table 9.1.

A simple manipulation of the reference S-N curve for amplitudes below the fatigue limit solves the formal insufficiency of a fixed slope of the reference S-N-curve given by the Miner modification by Haibach which leads to a fixed calculated fatigue lifetime curve between Miner original and Miner elementary. This newly introduced modification uses a parameter C in the description of the reference S-N curve. Any fatigue lifetime curve can be calculated varying the parameter C (Fig. 57).

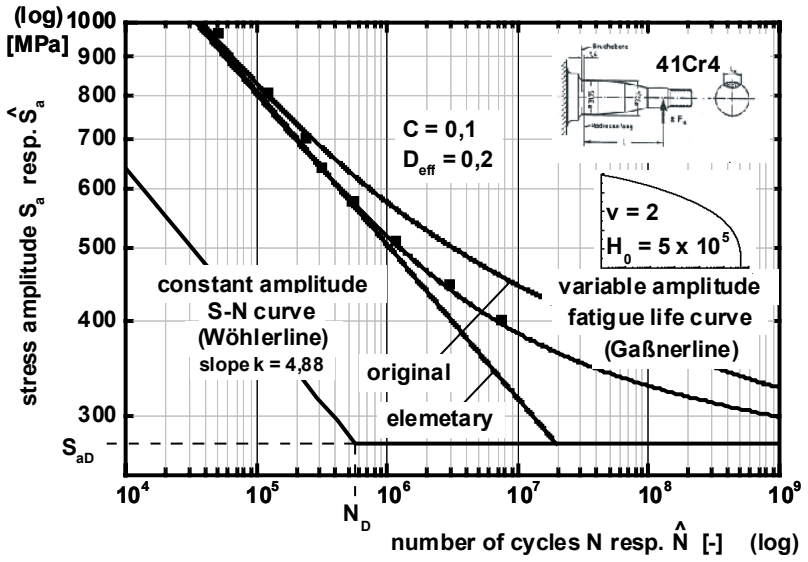

Fig. 58: Lifetime predictions using parameter C for a steel car axes.

Based on the reference S-N curve in accordance to the applied Miner modification a linear damage accumulation can be performed. For a stepped cumulative frequency distribution the linear damage accumulation can be calculated using the following equations:

$$D = \sum_i \frac{h_i}{N_i} \qquad N_i = N_D \cdot \left(\frac{S_{ai}}{S_{aD}} \right)^{-k^*} \tag{9.2}$$

The Miner modification by Hück uses an additional parameter C to adapt the form of the calculated fatigue lifetime curve. Therefore the calculated fatigue lifetime curve better fits the test results. In accordance to the assessment performed in [22-24] the test results have been recalculated evaluating the new modification. As an example the calculated fatigue life curve for a steel component specimen is given in figure 4. The $D_{eff} = \hat{N}_{exp} / \hat{N}_{calc}$ value is determined from experimental results at maximum stress amplitude value fare above the fatigue limit where the modifications elementary, original and Haibach deliver the same fatigue life and fit the evaluated experimental results best. The parameter C is adjusted to limit the error in the D_{eff} value for all test results.

Table 9.1: Miner rule modifications

	$S_a \geq S_{aD}$	$S_a < S_{aD}$
Original	$k^* = k$	$k^* = \infty$
Elementary	$k^* = k$	$k^* = k$
modified by Haibach	$k^* = k$	$k^* = 2\,k - 1$
modified by Liu/Zenner	$k^* = (k + m) / 2$	$S_a < ½\ S_{aD}$: $k^* = \infty$
modified by Hück	$k^* = k$	$k^* = k \cdot \left[1 + \frac{C}{\hat{S}_{ai} / S_{aD} - 1} \right]$

When the parameter C modification is used for lifetime prediction, the calculated lifetime in the high cycle regime increases. The main focus now is set upon an evaluation of influence parameters on the fatigue lifetime in the High Cycle Regime. The objective is to quantify recommended C and D_{eff} values for safe design life curve. An influence of the notch factor, the stress ratio and the slope of the S-N curve on the parameter C and the damage sum have been observed.

Used symbols: C: fit parameter; d: damage sum for a given stress level; D: damage sum; h: cycle frequency of a stress level; k: slope of the S-N curve; k*: slope of the reference S-N curve for damage accumulation; m: slope of the crack propagation S-N-curve, (m=3,6); ν: form parameter of the spectrum; N: number of cycles to failure (constant amplitude); $\hat{N}$: number of cycles to failure (variable amplitude); N_D: point of deflection of the S-N curve; S_a: stress amplitude; $\hat{S}a$: maximum value of the cumulative frequency distribution; S_{aD}: fatigue limit; i: stress level; eff: effective; calc.: calculated; exp.: experimental.

9.2 Experiments for Fatigue Life Prediction on Magnesium Alloys

H.-J. Ertelt, UST-ISD

In aircraft and automotive components, low weight is of great importance, if not a requirement. Because of the fact, that magnesium (Mg) possesses the lowest density of nearly all structural metals, both cast and wrought magnesium alloys have been developed for a variety of structural applications.

The cast magnesium AZ91 has dominated the magnesium alloy market to date. It is a low cost general – purpose alloy, limited to service below 130 ^oC to 160 ^oC because of the relatively small creep resistance. The introduction of rare earth (RE) in the Mg - alloys AE42, WE43 and RZ5 enables also creep resistance.

When using magnesium alloys in engineering design, fatigue life estimates are often needed, but up till now, industry is concerned about a serious void in fatigue data banks and models for magnesium alloys and processes.

To define some transfer functions of specimen fatigue data under constant amplitude tests to the component under spectrum loading, on the ISD a program has been started some years ago to define some significant cyclic material parameters of the Mg – alloy AZ91 and others for fatigue life prediction purposes.

For axial loading, smooth standard round die cast test bars were used with a diameter of 6.4 mm and as cast surface. The flat test bars for axial loading had a width of 10 mm and a thickness of 5 mm.

For the 3 – point – bending tests (3PB), flat cast specimens were used with a width of 9 mm and a thickness of 3 mm. The 3PB – tests were conducted at room temperature and at elevated temperature of 160 ^oC. The stress ratio R for the stress controlled constant amplitude tests for estimation of the S – N functions, was R = -1 and R = 0.1.

It could be observed, that the S – N curves show a “knee”, that means there is a marked change in the slope between high – cycle and endurance limit regimes, that can be used to determine a fatigue limit (fatigue strength). Similar to other metals, the fatigue strength of Mg – alloys seems to be dependent on the material tensile strength.

For the strain based cumulative damage approach the form of stress – strain hysteresis loops is of great importance. The test results show, that Mg – alloys seem to exhibit cyclic hardening. Furthermore, the cyclic stress – strain response of Mg – alloy AZ 91 for example shows, that the closed hysteresis loops become very “small” with increasing strain amplitudes. Normally, the unloading after a load reversal point in tension with coordinates ε_{max} and σ_{max} occurs with a slope of the tangent that represents the value of Young´s modulus (elastic unloading). In the case of the AZ91 tests this elastic part in the hysteresis loop after the load reversal point in tension vanish more and more with increasing strain amplitude. Furthermore the hysteresis loop becomes more and more asymmetric even in the stabilised case or better in the quasi – stabilised condition. In such a case, the application of the so called Masing - hypothesis for estimating the hysteresis loop for strain – based life prediction purposes (estimating the damage parameter), leads to an immense discrepancy between calculation and the reality.

Most of all fatigue test results, especially in the high – cycle – fatigue region show a wide scatter. Test bars with an extraordinary reduced fatigue life showed in most cases defects at the surface. Removing of the relatively rough as – cast surface of the specimen improved the fatigue properties of the test bars. A lot of test bars showed volumetric defects like cracks and material porosity . In round test bars in many cases circle shaped defects around the centre of the specimen were found. The variety of the different defects lead to a wide scatter of the test results.

At the moment the fatigue tests with the Mg – alloy AZ91 are concentrated to tests with notched specimens under constant amplitude tensile loading. After finishing these test series, it is planned to complete the tests by spectrum loading to define necessary transfer – functions for the strain – based cumulative damage approach of construction components.

10 REFERENCES

[1] Biallas, G., Dalle Donne, C. and Juricic, C: Monotonic and Cyclic Strength of Friction Stir Welded Aluminium Joints, *Advances in Mechanical Behaviour Plasticity and Damage, Proc. of EUROMAT 2000*, Vol. 1., D. Miannay, P. Costa, D. François (Eds.), Elsevier, 2000, pp. 115-120.

[2] Biallas, G. and Dalle Donne, C.: Reibrührschweißungen aus Aluminium charakterisieren, *Materialprüfung*, 42, 6, 2000, pp. 236-239.

[3] Braun, R., Biallas, G., Dalle Donne, C. and Staniek, G.: Characterisation of Mechanical Properties and Corrosion Performance of Friction Stir Welded AA6013 Sheet, *Materials for Transportation Technology EUROMAT '99 - Vol. 1*, Winkler, P.J. (Ed.), Wiley-VCH, 1999, pp. 150-155.

[4] Braun, R., Dalle Donne, C. and Staniek, G.: Laser Beam and Friction Stir Welding of 6013-T6 Aluminum Alloy Sheet, *Materialwissenschaft und Werkstofftechnik*, 31, 12, 2000, pp. 1017-1026.

[5] Dalle Donne, C., Biallas, G., Ghidini, T. and Raimbeaux, G.: Effect of Weld Imperfections and Residual Stresses on the Fatigue Crack Propagation in Friction Stir Welded Joints, *Second International Conference on Friction Stir Welding*, 2000, The Welding Institute, Abington Hall, UK, cd-rom.

[6] Dalle Donne, C. and Raimbeaux, G.: Residual Stress Effects on Fatigue Crack Propagation in Friction Stir Welds, *10th International Conference on Fracture, ICF 10*, Elsevier Science Publ., 2001, accepted for publication.

[7] Statische und Fatigue-Festigkeitsuntersuchungen an CFK-Bolzenverbindungen unter Raumtemperatur, IMA Test Report No. C 98/8, 1999.

[8] Bergner, F., Zouhar, G. and Tempus, G.: The material-dependent variability of fatigue crack growth rates of aluminium alloys in the Paris regime, *Int. J. Fatigue*, 23, 2001, pp. 383-394.

[9] Nocke, K., Bergner, F., Bersch, H., Haase, I., Worch, H., Tempus, G. and Loechelt, E.: Environment-sensitive fracture of aluminium alloy 6013, *Materials and Corrosion*, 51, 2000, pp. 628-634.

[10] Jägg, S.: PhD-Thesis, Universität Gesamthochschule Kassel, Institut für Werkstofftechnik und Metallische Werkstoffe, 1999.

[11] Hemptenmacher, J., Assler, H., Kumpfert, J. and Dudek, H.J: Fatigue damage mechanisms of titanium matrix composites, *ICCE6, Orlando, USA*, 1999, pp. 313-314.

[12] Peters, P.W.M., Assler, H., Hemptenmacher, J. and Xia, Z.: Fatigue of SCS-6/Timetal 834 at room temperature and 600°C, *ECCM 9 - Europ. Conf. on Comp. Mat., June 2000 ,Brighton, UK*,2000,

[13] Peters, P.W.M., Xia, Z., Hemptenmacher, J. and Assler, H: Influence of interfacial stress transfer on fatigue crack growth in SiC-fibre reinforced titanium alloys, *Composites*, Part A32, 2001, pp. 561-567.

[14] Hemptenmacher, J., Weber, K. and Peters, P.W.M: Ermüdung eines SiC(SCS-6)-Faser/Titan-Matrix Verbundwerk-stoffes bei 600°C und der Einfluss von Faser-Oxidation, *DGM Tagung Verbundwerkstoffe und Werkstoffverbunde, September 5-7, 2001, Chemnitz, Germany*,2001,

[15] Bartsch, M., Marci, G., Mull, K. and Sick, C.: Lifetime Prediction of Ceramic Thermal Barrier Coatings based on Lifetime Analyses of Close to Reality Tests, *Proceeding of 7th International Symp. on Ceramic Materials and Components for Engines, June 19-21, 2000, Goslar,*, Heinrich, J. and Aldinger, F. (Eds.), Wiley-VCH, 2001, pp. 285-290.

[16] Bartsch, M., Marci, G., Mull, K. and Sick, C.: Fatigue Testing of Ceramic Thermal Barrier Coatings for Gasturbine Blades, *Advanced Engineering Materials*, 2, 11, 1999, pp. 127-129.

[17] Bartsch, M., Marci, G., Mull, K. and Sick, C.: Damage Evolution of EB-PVD Thermal Barrier Coatings for Turbine Blades in Aircraft Engines under Close to Reality Testing Conditions, *International Journal of Materials and Product Technology*, 16, 1-3, 2001, pp. 248-257.

[18] Riedel, H.: *Fracture at High Temperatures*, Springer-Verlag, Berlin, 1987.

[19] Jung, A., Maier, H. J. and Christ, H.-J.: *Thermo-mechanical Fatigue Behavior of Materials, Third Volume, ASTM STP 1371*, Sehitoglu, H. and Maier, H.J. (Ed.), American Society for Testing and Materials, West Conshohocken, PA, 2000, S. 167-185.

[20] Staszewski, W.J., Biemans, C., Boller, C. and Tomlinson, G.R.: Impact Damage Detection in Composite Structures - Recent Advances, *Second International Workshop on Structural Health Monitoring, Stanford, California, USA, 8-10 September, 1999*,1999, pp. 754-763.

[21] Harris, C.M. [Ed.]: *Shock and Vibration Handbook*, McGraw-Hill Company, New York, 1987.

[22] Schütz, W. and Heuler, P.: Miner's Rule Revisited, *Materialprüfung*, 6, 2000, pp. 245-251.

[23] Eulitz, K.-G, Esderts, A., Kotte, K.L. and Zenner, H.: Lebensdauervorhersage I, *Forschungsheft 184, Forschungskuratorium Maschinenbau e.V., Frankfurt*, 1994, pp.

[24] Eulitz, K.-G, Döcke, H., Kotte, K.L. and Zenner, H.: Lebensdauervorhersage II, *Forschungsheft 227, Forschungskuratorium Maschinenbau e.V., Frankfurt*, 1997, pp.

[25] Haibach, E.: *Betriebsfestigkeit - Verfahren und Daten zur Bauteilberechnung*, VDI-Verlag GmbH, Düsseldorf, Germany, 1989.

[26] Zenner, H., Liu, J. and Sanetra, C.: Fatigue Behahiour under Uniaxial and Multiaxial Service Load, *Intern. Symposium on "Fatigue Damage Measurement and Evaluation under Complex Loadings, Fukuoka, Japan*,1991, pp. 120-125.

[27] Schütz, W., Bergmann, J. and Hück, M.: Relative Miner-Regel, IABG Report, Ottobrunn, 1988.